W.W. Hansen Laboratories

Stanford University

FINAL REPORT

INVESTIGATION OF OPTIMUM MAGNET GEOMETRIES FOR GAIN-EXPANDED FREE-ELECTRON LASERS

15 August, 1981 to 31 December, 1982

Air Force Contract Number: F 49620-81-C-0098

Principal Investigators

A.L. Schawlow
Professor of Physics
[redacted]

John M. Madey
Professor of Electrical Engineering
and High Energy Physics (Research)
[redacted]

November, 1983

UNCLASSIFIED
SECURITY CLASSIFICATION OF THIS PAGE

(10)

REPORT DOCUMENTATION PAGE

1a. REPORT SECURITY CLASSIFICATION: Unclassified	1b. RESTRICTIVE MARKINGS
2a. SECURITY CLASSIFICATION AUTHORITY	3. DISTRIBUTION/AVAILABILITY OF REPORT: Approved for public release; distribution unlimited
2b. DECLASSIFICATION/DOWNGRADING SCHEDULE	
4. PERFORMING ORGANIZATION REPORT NUMBER(S)	5. MONITORING ORGANIZATION REPORT NUMBER(S): AFOSR-TR- 83-1255
6a. NAME OF PERFORMING ORGANIZATION: Stanford University; 6b. OFFICE SYMBOL (If applicable)	7a. NAME OF MONITORING ORGANIZATION: AFOSR/NP
6c. ADDRESS (City, State and ZIP Code): Stanford, CA 94305-2184	7b. ADDRESS (City, State and ZIP Code): Bldg 410 Bolling AFB, DC 20332
8a. NAME OF FUNDING/SPONSORING ORGANIZATION: AFOSR; 8b. OFFICE SYMBOL (If applicable): NP	9. PROCUREMENT INSTRUMENT IDENTIFICATION NUMBER: F49620-81-C-0098
8c. ADDRESS (City, State and ZIP Code): Bolling AFB, Bldg. #410 Wash DC 20332	10. SOURCE OF FUNDING NOS.

PROGRAM ELEMENT NO.	PROJECT NO.	TASK NO.	WORK UNIT NO.
61102F	2301	A1	

11. TITLE (Include Security Classification): INVESTIGATION OF OPTIMUM MAGNET GEOMETRIES FOR GAIN-EXPANDED FREE-ELECTRON LASERS

12. PERSONAL AUTHOR(S): A.L. Schawlow, John M. Madey

13a. TYPE OF REPORT	13b. TIME COVERED	14. DATE OF REPORT (Yr., Mo., Day)	15. PAGE COUNT
Final	FROM 15 Aug 81 TO 31 Dec 82	Nov, 83	84

16. SUPPLEMENTARY NOTATION

17. COSATI CODES			18. SUBJECT TERMS (Continue on reverse if necessary and identify by block number)
FIELD	GROUP	SUB. GR.	

19. ABSTRACT (Continue on reverse if necessary and identify by block number)

The purpose of this research was the identification of the critical magnet and storage ring parameters for optimization of the efficiency, power output and gain of gain-expanded storag ring free elecetron lasers. While previous research had identified the basic properties of these devices, the approximations and simplifications employed in these efforts for solution of the equations of motion had led to some ambiguities which were not readily resolvable within the framework of the model employed. To resolve these ambiguities, a model was developed for the FEL wiggler magnet which permits an exact solution of the equations of motion. Using this model, numerical techniques have been employed to identify the dependence of the laser power output, gain, and efficiency on the magnet parameters.

20. DISTRIBUTION/AVAILABILITY OF ABSTRACT	21. ABSTRACT SECURITY CLASSIFICATION
UNCLASSIFIED/UNLIMITED ☒ SAME AS RPT. ☐ DTIC USERS ☐	Unclassified

22a. NAME OF RESPONSIBLE INDIVIDUAL	22b. TELEPHONE NUMBER (Include Area Code)	22c. OFFICE SYMBOL

DD FORM 1473, 83 APR EDITION OF 1 JAN 73 IS OBSOLETE.

Unclassified
SECURITY CLASSIFICATION OF THIS PAGE

TABLE OF CONTENTS

I. INTRODUCTION

The purpose of this research was the identification of the critical magnet and storage ring parameters for optimization of the efficiency, power output and gain of gain-expanded storage ring free electron lasers. While previous research had identified the basic properties of these devices, the approximations and simplifications employed in these efforts for solution of the equations of motion had led to some ambiguities which were not readily resolvable within the framework of the model employed.

To resolve these ambiguities, we have developed a model for the FEL wiggler magnet which permits an exact solution of the equations of motion. Using this model, we have employed numerical techniques to identify the dependence of the laser power output, gain, and efficiency on the magnet parameters. Using the same magnet model, Kroll, Rosenbluth and Wong have developed a series of analytic relations for the electrons' radiated energy spread and emittance. The Kroll, Rosenbluth and Wong results serve both as a cross-check to our numerical results, and as a means to extend considerations to cases not explicitly reviewed in our research.

Our research indicates that the most important parameters for gain-expanded storage ring FEL's in the low-extraction regime

is the betatron phase advance per period in the wiggler magnet, which should be as large as possible to optimize the power output and efficiency. In high extraction systems, the critical parameter is the damping time between laser shots. In quantitative terms, efficencies of the order of 2% appear possible using existing technology in the low extraction regime, while 4% appear attainable in the high extraction region. Advances in storage ring technology could raise the efficiency to beyond 10%. The optical amplification factors attainable with gain-expanded wigglers at these efficiencies are 10-100 times larger than attainable using a conventional wiggler magnet.

Background: The gain attainable in a FEL is typically a strong function of the electron current density. As an example, for optimized constant-period wigglers, the gain at long optical wavelengths is given by:[3]

$$G \sim 0.96 \times 10^{-4} \lambda^{3/2} \lambda^{1/2} (1 + a_w^2)^{1/2} \left[J_o \left(\frac{a_w^2}{1 + a_w^2} \right) - J_1 \left(\frac{a_w^2}{1 + a_w^2} \right) \right]^2 \frac{i}{(\beta\gamma\epsilon)^2} ,$$

where G = gain per pass

λ = wiggler period (cm)

λ = optical wavelength (cm)

$a_w^2 = K^2 = (\lambda\, eB/2\pi mc^2)^2$

B = wiggler RMS magnetic field (gauss)

$i/(\beta\gamma\epsilon)^2$ ≡ normalized current density

i ≡ electron current (amperes)

γmc^2 = electron energy (ergs)

ϵ = electron beam emittance (assumes equal vertical and horizontal emittance) (cm-rad)

while at short wavelengths, the gain can be approximated by:[4]

$$G \propto 3.9 \cdot 10^{-7} \frac{\lambda_0^{1/2} \lambda^{7/2}}{\epsilon_y^4} \left(\frac{\epsilon_y}{\epsilon_x}\right) \frac{(J_0 - J_1)^2}{\sqrt{1 + a_w^2}} \, i \, L$$

where ϵ_y = vertical emittance (cm-radians)

ϵ_x = horizontal (bend-plane) emittance

and we assume $\epsilon_x \geq \epsilon_y$. (1-2)

The long wavelength result (1-1) applies when the electron beam falls within the dimensions of the optical mode with which the e^- beam interacts, while the short wavelength results (1-2) applies when the e^- beam dimensions are larger than the optical mode.

In both the short and long wavelength limit, the current density $i/(\beta\gamma\epsilon)^2$ required for FEL operation increase systematically as an inverse function of the optical wavelength.

Other factors may also increase the current density required for FEL operation. In particular while the tapered-wiggler geometry offers the possibility of substantially improved efficiency, the variation in period or magnetic field required to enhance efficiency systematically reduces the small signal gain. The electron current required for such devices must therefore be raised over and above the values indicated in equations(1-1) and (1-2).

Since the current density for linear accelerators is typically fixed by the Lawson-Penner relation:[3]

$$\frac{\langle i \rangle}{(\beta\gamma\epsilon)^2} \lesssim 1.1 \times 10^4 \text{ amps/cm}^2 \qquad (1\text{-}3)$$

where $\langle i \rangle \equiv$ average electron current, operation of linac-based FEL's can be expected to become progressively more difficult as the desired laser wavelength is reduced from the infrared to the visible and ultraviolet spectral regions.

Substantially higher current densities can be obtained in electron storage rings in which synchrotron radiation damping actively reduces both the radius and angular divergence of the circulating electrons. Existing low-emittance storage rings[6] are believed operable at current densities $i/(\beta\gamma\epsilon)^2$ as large as 10^8 amperes/cm^2, higher by four orders of magnitude than the characteristic Lawson-Penner current density for linacs (1-3).

But to provide useful gain at high power, a storage ring based FEL must provide a means to cope with the electron energy spread induced by the interaction. For constant period wigglers, Renieri[7] has shown that the power output and efficiency of a SRFEL are determined by the relation:

$$\langle P_{laser} \rangle \approx \frac{\sigma_E}{E} \cdot P_{synch} \qquad (1\text{-}4)$$

where $\langle P_{laser} \rangle$ ≡ average laser power output

P_{synch} = net power radiated as incoherent synchrotron radiation

σ_E/E = fractional electron energy spread caused by laser operation,

and it is assumed that both the storage ring and the FEL wiggler have an energy acceptance comparable to or larger than the energy spread σ_E/E.

As is apparent from (1-4), operation of a SRFEL at high power and/or efficiency will require that both the storage ring and the FEL have a large energy acceptance. But, the only way to increase the energy acceptance of a constant period wiggler is to decrease the number of periods. Unfortunately, this step also reduces the gain, nullifying the storage ring's fundamental advantage in current density.

The gain expanded wiggler was proposed by Smith[8] as a solution to this dilemma for the storage ring FEL. By incorporating a transverse gradient in the magnetic field of the wiggler magnet, and dispersing the electrons in transverse position according to their energy, the gain can be made independent of energy spread. By increasing the gain attainable using an electron beam with a large energy spread, such a system could permit the power output of the SRFEL to be optimized without reducing the gain, thereby permitting high power operation at wavelengths unreachable using linear accelerator technology.

These possibilities encouraged several enquiries into the detailed properties of gain-expanded FEL's,.[1] Though less sensitive to energy spread than conventional FEL's, the gain-expanded FEL couples more strongly to the bend-plane emittance. The transverse acceptance of the gain-expanded wigglers, the laser-induced emittance growth, and the evolution of the emittance distribution in the ring must therefore be considered as key issues in the analysis of gain-expanded SRFEL performance.

In general, the early analyses assumed a sinusoidal wiggler field and developed the solutions to the "averaged" equations of motion for transverse position, energy, and optical phase. While these analyses revealed the basic features of operation, the use of the averaged equations of motion led to conflicting or ambiguous

results with respect to the laser-induced emittance growth. This study was undertaken to resolve these difficulties, and to provide specific guidance in the development of gain-expanded wigglers optimized for high-power operation.

Methodology : Since most of the difficulties of the earlier analyses of the gain-expanded FEL occurred as a consequency of the use of the averaged equation of motion, we chose to develop a model in which the exact equations of motion could be integrated directly, without penalties in computation time, and matrix methods used to characterize the basic transport properties of the wiggler. These objectives were satisfied through the use of a "thin-lens" model for the FEL wiggler, in which the individual magnets in the wiggler are represented as having a thickness small compared to their spacing, and electron motion between magnets is unaffected by the static magnetic field. The electrons motion between wiggler magnets can be integrated analytically in this model, while the computation of the angular deflection by the magnets requires knowledge only of the magnetic field at the point through which the electron passes.

Given this model, we examined the relationship between energy loss, energy spread, and emittance growth in both single pass operation and storage ring oeration. Where appropriate, we have compared these numerical results with the analytic experiments described by Kroll, Rosenbluth and Wang for operation in the small extraction region.

Finally, based on our numerical results and the analytic results of Kroll, Rosenbluth and Wang, we have identified the critical wiggler and storage ring parameters for optimization of gain-expanded SFREL power output, efficiency and gain, and have estimated the performance attainable in an optimized system.

In the following sections, we review the details of the model, the principal numerical results, the comparison with the analytic results of Kroll, Rosenbluth and Wang, the identification and role of the critical system parameters, and the characteristics of operation in the low and high extraction regimes.

II. DESCRIPTION OF THE MODEL

The storage ring FEL (SRFEL) system studied in this research is shown schematically in Figure 1. The system consists of (1) an FEL wiggler insertion, (2) the bulk of the storage ring (SR) transport line, and (3) an RF cavity which replenishes (on the average) the energy loss of the electron due to laser action and synchrotron radiation. The electron trajectories through this system were treated numerically in the energy, phase and bend-plane betatron coordinates x and x'.

To follow electron motion through the full SRFEL system the tracking program integrated the detailed equations of motion through the wiggler, then used the first-order transport matrix to propagate the electrons through the ring and RF cavity. To study the single-pass behavior of the wiggler, the programs followed the electron's motion only within the wiggler, starting with the specific desired initial conditions at the input to the wiggler, and concluding with the electron's coordinates at the end of the wiggler.

The key parameters for the FEL wiggler, storage ring and rf cavity are summarized in Table I. The FEL insertion is a split-magnet type, which employs two wiggler sections joined by a matching section in which $\mathcal{E} = 0$ (Fig. 2). Each wiggler section is a constant period array of discrete thin lens magnets. Quadrupole terms in the thin lenses supply the transverse gradient needed for gain expansion. The matching section provides for additional design parameters, which may be used to control the laser-induced betatron

excitation and energy spread. The thin lens model simplifies analytic and numerical calculations while retaining characteristics applicable to all transverse gradient wigglers.

1. The Thin Lens Wiggler Equations[9]

Each wiggler section consists of a lattice of repeated cells with period λ_o (Fig. 2(b)). The magnets are assumed to be "thin lenses" which produce a magnetic field $\underset{\sim}{B} = B(x)\hat{y}$ over an effective length Δz which is small compared to their separation $1/2\ \lambda$. The laser-off electron trajectories have constant slope $x' = \frac{dx}{dz}$ = tan θj between thin lenses j-1 and j. The deflection in x' at the j-th lens is

$$\sin\theta_{j+1} - \sin\theta_j = \frac{e}{\beta\gamma mc^2} B_j(x)\,\Delta z \qquad (2\text{-}1)$$

Nominal Trajectories: Orbits with mean position <x> = constant are sawtooth functions $\theta_{j+1} = -\theta_j = (-)^j\theta$ with amplitude X:

$$\sin\theta(\langle x\rangle) = -(-)^j \frac{e}{2\beta\gamma mc^2} B_j(\langle x\rangle + (-)^j X)\,\Delta z_j \qquad (2\text{-}2)$$

$$X(\langle x\rangle) = \frac{\lambda_o}{4}\tan\theta(\langle x\rangle)$$

$$= \frac{\lambda_o}{4}\left\{\frac{1-\beta_{\|}^2-\gamma^{-2}}{\beta_{\|}^2}\right\}^{\frac{1}{2}} \qquad (2\text{-}3)$$

where $\gamma = \gamma_o\ (1 + \langle x\rangle/\eta)$. For gain expansion, $\beta_{\|}$ should be

independent of <x> for nominal orbits, which gives the condition:

$$\frac{1}{\eta} = \frac{4}{\lambda_0} X' \beta^2 \gamma^2 \cos\theta \sin\theta \qquad (2\text{-}4)$$

In this study the thin lenses contain dipole and quadrupole contributions:

$$B_j(x)\,\Delta z_j = \alpha_j \left[1 + (x - X_j)/\beta_j\right] \qquad (2\text{-}5)$$

where $X_j = -(-)^j X(0)$. The constants α_j are determined from the $\gamma = \gamma_0$ orbit through Eqns. (2-2) and (2-3). Gain expansion through order $\beta_{11} = \beta_{11_0} + 0(\langle x\rangle^2)$ is obtained by choosing the $\beta_j = (B'_j/B_j)_{x=X_j}$ to satisfy Eqn. (2-4) at $\langle x\rangle = 0$. This solution is conveniently written in terms of the effective focal lengths f_j for $\langle x\rangle = 0$:

$$\begin{aligned} f_j^{-1} &= 2\beta_j \tan\theta \sec^2\theta \\ &= \frac{2}{\lambda_0}\left(\frac{X'_j}{1 + X'_j}\right)\hat{f}^{-1} \end{aligned} \qquad (2\text{-}6)$$

where $X'_j = -(-)^j X'(0)$ and

$$\hat{f}^{-1} = 4(\gamma_0^2 - 1)(1 - \beta_{11_0}^2)/\beta_{11_0}^2$$

is a dimensionless inverse focal length.

The wiggler cell structure is therefore determined by the parameters $\gamma_o, \beta_{\parallel o}, \lambda_o$ and X'.

Relation to $\tilde{\Lambda}$ and q: A general orbit will not maintain constant $< x >$ but will perform betatron oscillations as illustrated by Fig. 3. The transport matrix for $\begin{pmatrix} x \\ x' \end{pmatrix}$ through a single cell is written in terms of the focal lengths as

$$S = \begin{pmatrix} 1 - \lambda_o/2f_2 & \lambda_o/2 \\ -1/f_2 & 1 \end{pmatrix} \begin{pmatrix} 1 - \lambda_o/2f_1 & \lambda_o/2 \\ -1/f_1 & 1 \end{pmatrix}.$$

If the betatron period is M cells in length, then $S^M = 1$, and one finds

$$\cos(2\pi/M) = \cos(\lambda_o \tilde{\Lambda}) = 1 - \tfrac{1}{2}\left[\frac{1}{f_1} + \frac{1}{f_2} - \left(\frac{\lambda_o}{2}\right)^2 \frac{1}{f_1 f_2}\right].$$

The $< x >$ values for $f_{1,2}$ from Eqn.(2-6) relates the betatron phase advance per period $\lambda_o \tilde{\Lambda}$ to the f_j:

$$\hat{f}^{-1} = 2\left\{1 + \left[1 + \left(\frac{X'^2}{1 - X'^2}\right)\sin^2\left(\tfrac{1}{2}\lambda_o \tilde{\Lambda}\right)\right]^{\frac{1}{2}}\right\}$$

When $\lambda_o \tilde{\Lambda} \ll 1$ this simplifies to:

$$\tilde{\Lambda}^2 \simeq \frac{1}{\eta^2} \cdot \frac{1-\beta_{\parallel_o}^2}{1-X'^2} .$$

The nominal optical phase advance is

$$q = \frac{2\pi}{\lambda}\left(\frac{1}{\beta_{\parallel_o}} - 1\right) \simeq \frac{\pi}{\lambda}(1-\beta_{\parallel_o}^2)$$

where λ is the operating wavelength.

The above relations can be used to determine the wiggler cell from q, $\tilde{\Lambda}$, λ, λ_o and X'. In the split-magnet design, these parameters may be independently specified for the two sections. The first and last cell in each section are set at half strength to better match trajectories into the FEL.

Laser-On Equations of Motion: At each thin lens, the orbit is deflected according to Eqn. (2-1). Between the lenses the radiation field is

$$\underset{\sim}{a}_s = (\mathcal{E}/k)\cos(\omega t - kz + \phi_o)\,\hat{x} \qquad (2\text{-}7)$$

so the Lorentz force on the electron is

$$\frac{d}{dt}(\gamma mc\beta_\perp) = -e[\mathcal{E}_x - \beta_\parallel B_y] = e\mathcal{E}(1-\beta_\parallel)\sin\psi$$

$$\frac{d}{dt}(\gamma mc^2) = -e\beta_\perp c\mathcal{E}_x = e\mathcal{E}\beta_\perp c\sin\psi$$

$$\psi = \omega t - kz + \phi_o \qquad (2\text{-}8)$$

$$\gamma^{-2} = 1-\beta^2 = 1-\beta_\perp^2-\beta_\parallel^2$$

The first of these may be integrated at once

$$\beta_\perp \gamma = (\beta_\perp \gamma)_0 - \frac{e\mathcal{E}}{\omega mc^2}(\cos\psi - \cos\psi_0). \tag{2-9}$$

Hence, x, γ, ψ satisfy the coupled system

$$\begin{aligned} \frac{dx}{dz} &= \frac{\beta_\perp}{\beta_\parallel} \\ \frac{d\gamma}{dz} &= \frac{\beta_\perp}{\beta_\parallel} \cdot \frac{e\mathcal{E}}{mc^2}\sin\psi \\ \frac{d\psi}{dz} &= k\left(\frac{1-\beta_\parallel}{\beta_\parallel}\right) \end{aligned} \tag{2-10}$$

where $\beta_\parallel, \beta_\perp$ and $x' = \beta_\perp/\beta_{\perp\perp}$ are known through (2-8) and (2-9).

2. a_s Correction on Entry or Exit

On entering the laser-field region from a field-free region the trajectory slope undergoes a correction resulting from the fact that the canonical and kinetic momenta differ by the vector potential term (Fig. 4). If the field is given by Eqn. (2-7) for $x > 0$, then by conserving both components of $\gamma mc\underline{\beta} - e\,\underline{a}_s/c$ across the boundary

$$\Delta x' = \pm \frac{1}{(\gamma\beta_\parallel)} \cdot \frac{e\hat{a}_s}{mc^2}\cos\psi \tag{2-11}$$

where ± applies to the cases of entering and exiting from the field respectively.

Since the field build-up must take place over a finite region $\delta\ell$, there is actually some $-e\underset{\sim}{v} \cdot \underset{\sim}{\varepsilon}$ energy loss as well. This can be estimated by considering the field produced by two oscillating current sheets

$$\underset{\sim}{J} \propto e^{+i\omega t}\left[\delta(z) + e^{i\varphi}\,\delta(z-\delta\ell)\right]\hat{x}$$

with $-\Delta\phi = k \cdot \delta\ell = \pi/2$. This generates a field $\varepsilon = 0$ for $z < 0$, a standing wave for $0 < z < \delta\ell$, and a travelling wave like Eqn. (2-7) for $z > \delta\ell$. Integrating the work done on the electron from 0 to $\delta\ell$ for a trajectory $x' = \text{const.}$ results in

$$\Delta\gamma = \mp\, x' \,\frac{eQ_s k}{mc^2}\left(\frac{\pi}{4}\sin\psi - \frac{1}{2}\cos\psi\right).$$

3. Matching Section

The first-order transformation matrix for a transport line of static magnetic fields is customarily written[10]

$$\begin{pmatrix} x \\ x' \\ \ell \\ \delta \end{pmatrix}_s = \overbrace{\begin{pmatrix} r_{11} & r_{12} & 0 & r_{14} \\ r_{21} & r_{22} & 0 & r_{24} \\ r_{31} & r_{32} & 1 & r_{34} \\ 0 & 0 & 0 & 1 \end{pmatrix}}^{R} \begin{pmatrix} x \\ x' \\ \ell \\ \delta \end{pmatrix}_1 \qquad (2\text{-}12)$$

where x,x' are the transverse position and slope, ℓ is the trajectory path length difference from the nominal orbit, and δ is the fractional energy deviation $(E - E_o)/E_o$ from the nominal energy. The functions in the upper left-hand block are written in terms of the betatron function $\beta(s)$ and betatron phase $\phi(s)$ (where $\phi'(s) = \frac{1}{\beta(s)}$):

$$r_{11} = \sqrt{\beta(s)/\beta(o)}\cos\phi \qquad r_{12} = \sqrt{\beta(s)\beta(o)}\sin\phi$$
$$r_{12} = r_{11}' \qquad r_{22} = r_{12}' \tag{2-13}$$

and $r_{11}r_{22} - r_{12}r_{21} = 1$. There is also the general relation[11]

$$\begin{pmatrix} r_{31} \\ r_{32} \end{pmatrix} = \begin{pmatrix} -r_{21} & r_{11} \\ -r_{22} & r_{12} \end{pmatrix} \begin{pmatrix} r_{14} \\ r_{24} \end{pmatrix} \tag{2-14}$$

The transformation

$$H_s = \begin{pmatrix} 1 & 0 & 0 & -\eta(s) \\ 0 & 1 & 0 & 0 \\ 0 & 0 & 1 & 0 \\ 0 & 0 & 0 & 1 \end{pmatrix} \tag{2-15}$$

brings one to the betatron coordinate $x_\beta = x - \eta\delta$. Since $x_\beta = x'_\beta = 0$ is a constant for any nominal orbit, the 14- and 24- components or $R_\beta = H_s R H_o^{-1}$ must vanish. This establishes two more relations

$$\begin{aligned} r_{14} &= \eta(s) - r_{11}\,\eta(0) \\ r_{24} &= \eta(0)\, r_{21} \end{aligned} \qquad (2\text{-}16)$$

In the non-saturated regime, an on-axis beam is excited by the laser into an ellipse in x_β , x'_β phase space whose aspect ratio and inclination determine the betatron function $\beta(s)$ and $\beta'(s)$ and whose area is the emittance A. Each position on this emittance ellipse corresponds to an entering on-axis electron with a given initial optical phase. A transformation of the form of Eqns. (2-12) to (2-15) will rotate the ellipse at the matching section through an angle $\Delta\phi_m = \phi(s) - \phi(0)$ together with a change of scales according to $\beta(0)$ and $\beta(s)$. The phase space area is invariant since detR = 1.

In addition to the above relations, which apply to transport lines in general, the following conditions are probably desirable for the matching section in a split-magnet FEL:

(1) In order to connect nominal orbits, require $\eta(0)=\eta_1$ and $\eta(s) = \eta_2$ be given in terms of the wiggler parameters through Eqn. (2-4)

(2) The transverse beam size in the second section will

be most compact if $\beta(0) = \beta_1$ and $\beta(s) = \beta_2$ and their derivaties match the intrinsic β functions for the two sections.

3. The optical phase shift between sections is:

$$\Delta\psi = \omega(L_m + \ell(s) - \ell(0))/\beta c$$
$$= \Delta\psi_m + k(\ell(s) - \ell(0))/\beta \qquad (2\text{-}17)$$

where L_m and $\Delta\psi_m$ are the nominal path length and optical phase advance. For gain expansion in the second section, it is sufficient that the transport be isochronous in the sense $\frac{\partial}{\partial\delta}(\Delta\psi) = 0$. Using Eqn. (2-17) and the 34-component of R_β to find the energy dependence of $\ell(s) - \ell(0)$, this condition is equivalent to:

$$\eta_1 r_{31} + r_{34} = L_m/\beta^2\gamma^2 . \qquad (2\text{-}18)$$

4. Storage Ring Transformation Matrix

The general transformation from s=C to s=A in Fig. 1 is again a matrix R as in Eqn. (2-12) as long as damping is ignored. Damping is introduced by altering the betatron transformation $R_\beta = H_A R H_C^{-1}$ to $R_{\beta d} = B_d R_\beta$, where

$$B_d = \begin{pmatrix} A_x & 0 & 0 & 0 \\ 0 & A_x & 0 & 0 \\ 0 & 0 & 1 & 0 \\ 0 & 0 & 0 & A_E \end{pmatrix}$$

and A_x, A_E are the betatron amplitude and energy damping coefficients discussed below. The total transformation matrix with damping is then $R_d = H_A^{-1} R_{\beta d} H_C$:

$$R_d = \begin{pmatrix} A_x r_{11} & A_x r_{12} & 0 & A_x(r_{14} - \eta_A) + \eta_A A_E \\ A_x r_{21} & A_x r_{22} & 0 & A_x r_{24} \\ r_{31} & r_{32} & 1 & r_{34} \\ 0 & 0 & 0 & A_E \end{pmatrix}$$

The damping coefficients are (see ch. IV of ref. 10):

$$A_E = \frac{1 - U^o_{syn}\ (2 + D)}{1 - U^o_{syn}}$$

$$A_x = 1 + \frac{1}{2} D\ U^o_{syn}$$

where U^o_{syn} is nominal fractional energy loss E_{syn}/E_o per turn due to synchrotron radiation and D is the damping partition parameter. The characteristic number of turns to damp is $N_D = 1/U^o_{syn}$. The matrix element r_{34} is αL_r, where α is the momentum compaction factor and L_r is the ring circumference traversed from C to A.

Using the equations in this and in the previous section we find that the betatron phase advance over the ring $\Delta\phi_r$ together with $\beta(A) = \beta_1, \beta(C) = \beta_2$, $\eta(A) = \eta_1$, $\eta(C) = \eta_2$, A_x, A_E, α and L_r fully characterize the storage ring by determining all the coefficients of R_d. The ring tune ν_x is the total number of betatron periods per turn

$$\nu_x = \frac{1}{2\pi}\left[(\tilde{\Lambda}L)_1 + \Delta\phi_m + (\tilde{\Lambda}L)_2 + L\dot{p}_r\right].$$

5. RF Accelerating Cavity

The RF cavity provides a purely longitudinal acceleration so that the electron's energy and slope are changed according to[10]

$$\gamma_c - \gamma_B = \gamma_0 U^0_{rf} \cos\theta_{rf}$$

$$x'_c = x'_B\left[1 - \frac{\gamma_c - \gamma_B}{\gamma_B}\right] \qquad (2\text{-}20)$$

where U^0_{rf} is the RF voltage and $\theta_{rf} = \omega_{rf} \cdot t$ is the RF phase. The change in RF phase over the ring is

$$\Delta\theta_{rf} = \frac{2\pi}{L_r}\left\{x r_{31} + x' r_{32} + \alpha L_r \delta\right\} \qquad (2\text{-}21)$$

where x, x', δ refer to the previous orbit values, and r_{31}, r_{32}, α, L_r are the ring parameters defined above. In Eqn. (2-21) ω_{rf} has been taken to equal the revolution frequency (a higher harmonic must be used for multiple bunch operation).

III. TEST OF GAIN-SPREAD-EXCITATION RELATIONS

In a transport line without damping, electrons advance in betatron phase about the perimeter of an x_β , x'_β phase space ellipse whose area A is an invariant (the emittance).* In storage ring operation, A is exponentially damped over many turns due to radiation damping, a combined effect of synchrotron radiation in the bends and the longitudinal momentum gain in the RF cavity. In steady-state, this is balanced by the emittance excitation due to quantum fluctuations.

It is important to know what effect the laser insertion has on the emittance and energy of an electron, since the ring can recirculate only those particles which lie within an acceptance set by physical apertures. If E_0, A_0 are input energy and emittance, and E, A are their values at the laser output, one may expand in powers of the laser field

$$E \simeq E_o + E_1 + E_2$$
$$A \simeq A_o + A_1 + A_2 \qquad (3\text{-}1)$$

---

* We use A in this report to designate the area enclosed by the x - x' phase space ellipse. This differs by a factor of π from ϵ, the product of the beam radius and angular divergence frequently used as an alternative definition of the emittance, and is 2π times the invariant J defined by Kroll and Rosbenbluth.[12]

where E_i, $A_i \sim \varepsilon^i$. Kroll and Rosenbluth[12] have shown that the gain-spread-excitation (GSE) relations

$$\langle E_2 \rangle = \frac{1}{2} \frac{\partial}{\partial E_0} \langle E_1^2 \rangle + \frac{1}{2} \frac{\partial}{\partial A_0} \langle E_1 A_1 \rangle$$
$$\langle A_2 \rangle = \frac{1}{2} \frac{\partial}{\partial A_0} \langle A_1^2 \rangle + \frac{1}{2} \frac{\partial}{\partial E_0} \langle E_1 A_1 \rangle \qquad (3\text{-}2)$$

hold in the small signal limit under very general circumstances. The averages are made over both betatron phase and initial optical phase.

When the FEL excitation is dominated by terms in the hamiltonian near a single harmonic m of the betatron oscillation, one obtains the Manley-Rowe relation

$$\langle \Delta A \rangle = -m\lambda \langle \Delta \delta \rangle \qquad (3\text{-}3)$$

where $\Delta A = A - A_0$, $\Delta \delta = (E - E_0)/E_0$.

The fundamental formulae Eqn. (3-2) and (3-3) were explored numerically. First the output emittance ellipse parameters β and β' were established from a distribution of electrons entering on-axis at different optical phases. This determined A as a

function of the output x_β , x'_β for a single electron. For each input condition, the output was calculated at two values of the laser field ε in order to decompose E and A into the first and second-order terms of Eqn. (3-1). The phase averaging was accomplished by dividing the range from 0 to 2π into N_ϕ (or N_ψ) equally spaced betatron (or optical) phase angles. The total ΔA in Eqn. (3-3) is just the area of a plane figure, and was computed directly by cubic spline integration, which has the advantage of not introducing errors due to distortion of the emittance figure from its initially determined (on-axis) elliptical form β, β' .

For this study, the two wiggler sections were chosen to be the same, and the matching section transformation was the identity.

In all cases tested, Eqns.(3-2) were verified, up to the precision of the numerical methods. Two representative cases are listed in Table II. The first case is typified by transverse gradient wigglers dominated by m = 1. The energy derivative GSE terms are negligible and the Manley-Rowe relation holds. The second example was constructed for a non-negligible m = 0 contribution by making qL and $\gamma\lambda_o$ small. In this case the first GSE relation has a noticeable energy-derivative terms, and there is an additional emittance growth about 8% larger beyond that predicted by Eqn. (3-3).

The a_s correction described in the previous section is important even at low fields. This is demonstrated by the results of Table III, where the Manley-Rowe relation is examined when the a_s correction is

applied with the wrong phase or omitted entirely. This causes the emittance excitation, which is correctly given by Eqn. (3-3) to be underestimated.

IV. MONTE CARLO-SIMULATIONS (LOW EXTRACTION)

1. Description of the Simulation.

A Monte Carlo technique was used to investigate the equilibrium energy and emittance distributions in the low extraction regime in which the GSE relations apply. In this simulation, the transformations from section II were applied to propagate a single electron repeatedly through the SRFEL. According to the ergodic theorem, a histogram of the single-electron energy or emittance values after many passes should give the equilibrium distribution for a circulating electron bunch. Of course, this neglects electron-electron interactions (such as space charge and wake field effects) which are known to be important at high current.

Because the ring is not isochronous, the electron's arrival time at the laser insertion is essentially uncorrelated with the rapidly varying optical phase. In the simulation, the initial optical phase ψ_o in Eqn. (2-7) was treated as a stochastic variable and was chosen randomly in $(0, 2\pi)$ for each pass. A longitudinal optical pulse shape may be accounted for by letting the amplitude ε in Eqn. (2-7) depend upon time. We assume that the laser resonator length is turned so that an optical pulse is coincident with the electron bunch on each pass (a general scheme might allow for more than one electron and/or optical bunches). Then ε is a function of the electron's RF phase θ_{rf}. For this study, a gaussian pulse

$$\mathcal{E} = \mathcal{E}_o \exp\{-(\theta_{rf} - \theta_s)^2/2\sigma_\theta^2\}$$

was used, where θ_s is the synchronous RF phase. A cw pulse is simulated by taking $\sigma_\theta >> 2\pi$.

2. Convergence

The characteristic time scale over which an electron's position in phase space remains correlated is given by the number of turns to damp N_D . That is to say, a many-particle bunch will achieve its equilibrium distribution after a few damping times. For the single particle simulation, this means that N_D turns are required to explore each region of phase space. It was found that 40 damping times was sufficient for two digit accuracy in moments of the distribution. This is demonstrated by Fig. 5, which plots one such derived value over the length of the simulation. Six simulation runs are illustrated, three of which have been run to 80 damping times. They differ only in the choice of the initial electron coordinates or the seed value used to generate the uniform distribution for the stochastic variable ψ_o . Computation time becomes prohibitive for simulation runs much longer than this.

3. Energy and Emittance Distributions

The equilibrium energy distribution due to quantum fluctuations in a normal storage ring is gaussian. This was also found to be true in our simulations, as illustrated in Fig. 6. Note, however, that in many cases the gaussian was modulated near the central maximum by two symmetrically placed peaks. The depleted region between them does not in general correspond in

RF phase to the optical pulse width, and has been seen for CW operation as well (Fig. 7). But in all cases, the wings of the distribution were found to retain the gaussian form. This is important, since the beam lifetime would be reduced if the distribution approached zero more slowly.

The electrons' emittance distributions showed a generally smooth fall-off from a maximum at zero or slightly off-axis (Fig. 8). Structure off-axis was a frequent feature of the simulation runs, but was not found to be correlated from run to run.

4. Extracted Energy vs. Energy Spread

The width of the energy distribution, as given by its standard deviation σ_δ is important since even for gain-expanded wigglers the ring energy acceptance sets an upper limit on the allowable energy spread. As can be seen from Fig. 9 (wiggler parameters: $qL = \lambda L = 8\pi$, $1-X'^2 = .99$, $L = 20$ m; cw optical pulse, $\lambda = 1$ μm); the extracted energy is proportional to the energy spread for laser intensities below saturation. This may be expressed as the ratio

$$\text{"efficiency ratio"} = -\langle \Delta\delta_{laser} \rangle N_D/\sigma_\delta = P_{laser}/\sigma_\delta \, P_{synchrotron} \qquad (4\text{-}1)$$

where $P_{laser} = -\langle \Delta\delta_{laser} \rangle E_o I$. The efficiency ratio below saturation for the example of Fig. 9 is ~ 1.5, as estimated by Kroll and Rosenbluth.[12]

5. Extracted Energy vs. Emittance

The laser must not induce emittance growth which exceeds the acceptance of the storage ring. Below saturation, Kroll[13] has shown that the mean emittance $< A >$ is proportional to the laser extracted energy

$$\langle A \rangle = - \left(\frac{N_D}{1 - D} \right) \lambda \langle \Delta \delta_{laser} \rangle . \qquad (4\text{-}2)$$

This has been verified by the numerical simulations, as shown in Fig. 10 (same wiggler parameters as for Fig. 9). The bend plane acceptance for a TGW has been estimated.[14] For a thin lens wiggler this sets a limit on the emittance A of

$$A \simeq \frac{\lambda}{8\pi} (\lambda_0 \tilde{\Lambda}) \qquad (4\text{-}3)$$

For the conditions of Fig. 10, this predicts saturation at $< A > \approx 2.5 \times 10^{-6} \pi$ cm-rad, in agreement with the simulation results.

6. Efficiency vs. Damping Partition

According to Robinson's theorem, the total damping between the energy and transverse dimensions is a constant specified by N_D. This may be written in terms of the partition parameter D

$$J_E + J_x = 3$$

where

$$J_E = 2 + D$$

$$J_x = 1 - D.$$

For "separated-function" storage rings the energy damping is normally twice the transverse damping (D=0). We explored the idea of adjusting D to control the laser-induced emittance growth. As D approaches -2 the energy spread grows, while the $D \to 1$ limit kills the gain. Kroll and Rosenbluth[15] have shown that the efficiency ratio of Eqn. (4-1) for a cw optical beam is a parabola with a maximum at equal damping in both dimensions ($D = -\frac{1}{2}$). This behavior is generally confirmed in the unsaturated regime by the Monte Carlo results (Fig. 11). At saturated power levels the parabolic shape is deformed and has a peak usually near $D = 0$.

The results for short optical pulses are generally similar and indicate best operation for $-1 < D < 0$. There is evidence for a shift in the optimal operating point towards greater transverse damping at higher power densities (Fig. 12).

7. Efficiency vs. Betatron Phase Advance

Figure 13 is a plot of the efficiency ratio vs. λ_L with the number of periods L/λ_o held fixed. The three curves are for different values of X'. The detailed behavior is complicated, but the efficiency is seen to be relatively insensitive to λ_L as long as $\Lambda\lambda_o$ does not approach π, where the wiggler orbits become unstable.

8. Wiggler with Odd-π Phase Advance

The simulation showed essentially no difference between operation at even and odd multiples of π betatron phase advance, as shown by the comparison of Table IV.

V. POWER OUTPUT AND GAIN OF OPTIMIZED LOW EXTRACTION GAIN-EXPANDED SRFEL's

The research on the relation of radiated energy $<\delta>$, energy spread $<\delta^2>$ and emittance $< A >$ in low extraction gain-expanded SRFEL's indicates two basic saturation mechanisms, emittance growth and energy-spread accumulation. Emittance growth will result in saturation of the radiated energy per electron if the emittance exceeds the finite acceptance of the gain-expanded wiggler, while energy spread accumulation will result in loss of the net electron current if the energy spread exceeds the acceptance of the ring. As discussed below, these saturation mechanisms can be minimized by operation of a high betatron phase advance per period, a negative damping partition function $D \simeq -0.5$, and a large storage ring energy acceptance.

From equation (4-2) and Figure 10, the mean emittance and radiated energy in a gain-expanded SRFEL at low power are related as

$$< A > = - \frac{\lambda}{1 - D} \frac{< \delta >}{\mu^{\circ}_{sym}} \qquad (4\text{-}2)$$

But as the mean radiated energy $<\delta>$ increases, the emittance $< A >$ will eventually approach the transverse acceptance of the wiggler, at which point the radiated energy will fall. Assuming a limiting emittance $< A >$ equal to the wiggler acceptance as defined in Eq. (4-3),

we obtain the emittance-induced upper limit to $\langle\delta\rangle$

$$\langle\delta\rangle \leq -u^{\circ}_{syn}\,(1-D)\,\frac{\lambda_0\tilde{\Lambda}}{3\pi} \qquad (5\text{-}1)$$

To secure the largest possible value of radiated energy $\langle\delta\rangle$ and efficiency $\langle\delta\rangle / u^{\circ}_{syn}$, equation (5-1) indicates that we should operate at the largest possible value of betatron phase advance/period $\lambda_0\tilde{\Lambda}$ and a large negative value of D. From Figure 13, the betatron phase advance per period is limited to values less than 0.8 to insure stability. Assuming a maximum betatron phase advance $\lambda_0\tilde{\Lambda} \sim 3\pi/4$ and D = - 0.5, we obtain an upper limit to $\langle\delta\rangle/u^{\circ}_{syn}$:

$$\frac{\langle\delta\rangle}{u^{\circ}_{syn}} \leq \frac{4.5}{32} \sim 14\% \qquad (5\text{-}2)$$

While higher values of efficiency could be obtained by using a more negative value of D, such a choice would increase the energy spread as discussed below, which would likely set an independent upper limit to the radiated power below that allowed by (5-2).

With respect to the energy spread, the theoretical and numerical analysis of the relation of energy spread and radiated energy indicate a relationship of the form:

$$\frac{\langle\delta\rangle}{u^{\circ}_{syn}} = F(D)\cdot\sigma_{\varepsilon} \qquad (5\text{-}3)$$

where the maximum value of the function F occurs near D ≃ - 0.5, F(-0.5) = 1.5. If the system is actually operated at the radiated energy allowed by (5-1), the storage ring must have an energy acceptance compatible with the spread σ_δ indicated by (5-3), eg:

$$\sigma_\delta \simeq \frac{1-D}{F(D)} \cdot \frac{\lambda_o \bar{\lambda}}{8\pi} \qquad (5\text{-}4)$$

$$\simeq 10\% \text{ for } \lambda_o \bar{\lambda} = 3\pi/4 \,, \; D = -0.5$$

For steady state operation, the storage ring acceptance must exceed the energy spread σ_δ by a factor of four to six to assure an adequate lifetime (as electrons outside the energy acceptance of a storage ring are generally quickly lost). For the 10% energy spread computed in Eqn. (5-4), this would require an acceptance of the order of ± 40-60%, a number which exceeds the acceptance of existing ring designs by an order of magnitude.

Whether it will be possible to design rings with an energy acceptance adequate to take advantage of the power output allowed by Eqn. (5-1) is not presently known. For rings of smaller acceptance, the allowable FEL power output can be computed from (5-3). Assuming a partition function D ≃ -0.5 and an upper limit to the energy spread σ_δ equal to 1/6th the storage ring acceptance, we obtain:

$$\frac{\langle \delta \rangle}{u^\circ_{syn}} \sim \frac{1}{4} \cdot (\text{Storage Ring fractional energy acceptance}) \qquad (5\text{-}5)$$

Assuming a fractional energy acceptance $\approx 8\%$, as in the LEDA ring design developed at Frascati,[16] a laser power output equal approximately to 2% of the synchrotron radiation could be obtained.

As discussed in the next section, a higher energy spread σ_δ may be allowable in transient operation in the high-extraction regime if the non-gaussian nature of the electron distribution function is exploited to permit operation at an energy spread more nearly equal to the storage ring acceptance.

Gain: Given that the initial rational for the gain-expanded SRFEL was the desire to optimize the gain of high-acceptance SRFEL's, it is appropriate to determine the extent to which the gain-expanded system actually accomplishes this purpose. As discussed below, a comparison of the gain attainable in conventional and gain-expanded wigglers of equal acceptance indicates that this objective has, in fact, been achieved.

The energy acceptance of conventional, constant period wigglers is determined by the number of periods. Inspection of the width of the gain curve indicates that, allowing for a 50% reduction in gain, the acceptance of a conventional constant-period wiggler is

$$\sigma_\delta \sim \frac{0.2}{N} \qquad (5\text{-}6)$$

where $N \equiv L/\lambda_o$ is the number of magnet periods. Assuming the optimum optical mode size, the small signal gain of such a wiggler can be expressed in terms of the acceptance as:

$$G_{conv}^{max} \approx 1.7 \times 10^{-4} \; i \; \frac{a_w^2}{1+a_w^2} \; \frac{1}{\gamma_o} \; \frac{1}{\sigma_\delta^2} \left[J_o\left(\frac{1}{2}\frac{a_w^2}{1+a_w^2}\right) - J_1\left(\frac{1}{2}\frac{a_w^2}{1+a_w^2}\right)\right]^2 \tag{5-7}$$

For a gain-expanded wiggler, maximum gain is attained if the net optical phase slip qL is set equal to the net betatron phase advance L:

$$G_{Gx}^{max} \approx 1.6 \times 10^{-2} \; i \; \frac{a_w^2}{1+a_w^2} \; \frac{N_{Gx}}{\lambda_o \tilde{\Lambda}} \; \frac{1}{\gamma_o} \left[J_o - J_1 \right]^2 \tag{5-8}$$

Where N_{Gx} is the number of periods in the gain-expanded wiggler and the optimum optical mode area has been assumed. Assuming that the betatron phase advance per period $\lambda_o \tilde{\Lambda}$ is selected using Eqn. (5-4) to provide an energy acceptance just equal to σ_δ, the gain of the gain-expanded wiggler can also be expressed in terms of the energy spread:

$$G_{Gx}^{max} \approx 6.4 \times 10^{-4} \; i \; \frac{a_w^2}{1+a_w^2} \; \frac{N_{Gx}}{\sigma_\delta} \; \frac{1}{\gamma_o} \left[J_o - J_1 \right]^2 \tag{5-9}$$

For equal electron energies, γ_o energy acceptances σ_δ, and normalized wiggler magnetic fields $\alpha^2\beta^2$, the ratio of the gain attainable in the gain-expanded wiggler to the gain of the conventional wiggler is therefore simply:

$$\frac{G_{Gx}^{max}}{G_{conv}^{max}} \approx \frac{6.4}{1.7} \cdot N_{Gx} \cdot \sigma_\delta \qquad (5\text{-}10)$$

From equation (5-10) we see that the gain-expanded wiggler will generally provide superior gain when the energy spread σ_δ is large and conditions permit the maximization of the number of periods of the gain-expanded wiggler. As an example, if $N_{Gx} = 40$ and $\sigma_\delta = 5\%$, equation (5-10) yields

$$\frac{G_{Gx}^{max}}{G_{Conv}^{max}} = 7.5$$

In this example, the gain-expanded wiggler would provide a gain almost an order of magnitude higher than available using a conventional wiggler.

As discussed further in the next section, somewhat higher gain advantages may be possible if the gain-expanded system is operated in the high-extraction regime in which smaller values of $\lambda_o \tilde{\Lambda}$ can be used than those allowed by Eqn. (5-4).

VI. HIGH EXTRACTION OPERATION

While the preceeding sections of this report have dealt with the characteristics of gain-expanded SRFEL operation at radiated energies per pass which are small compared to $\gamma_o mc^2$ the properties of these systems at high radiated energy per pass are also potentially interesting. In the high extraction regime, high power is achieved by pusling the laser the order of once every damping time. This intermittent mode of operation should permit extraction of a significant fraction of the electron's energy in each pulse with good optical gain and an energy distribution function with significantly improved statistics as compared to the gaussian distribution function characteristics of the low-extraction regime. For a given storage ring energy aperture, operation at high extraction may permit a factor of two higher power output and efficiency than operation at low extraction.

The characteristics of the laser interaction in the high-extraction regime are illustrated in Table V and Figures 14-16. Table V indicates the dependence of radiated energy per pass on optical power density for a thin-lens gain-expanded wiggler operating at resonance $\hat{\gamma}L = \tilde{\Lambda}L = 4\pi$ assuming a zero-emittance electron beam. At these values of $\tilde{\Gamma}L$ and $\hat{\gamma}L$, the wiggler operates in the m=1 mode in which the gain and electron statistics are independent of initial energy. The effects of finite initial emittance are illustrated in Figures 14-16.

As is apparent in Table V, the power density for gain saturation in gain-expanded wigglers can be very high. In this example, gain saturation occurs at an extraction of 8% of the initial electron energy, at which point the optical gain is reduced by 50%. This behavior has been discussed in the previously published description of the gain-expanded wiggler.[17]

The high power saturation characteristics of the gain expanded wiggler conveys the same advantage in the high extraction regime as its large energy acceptance conveyed in the low-extraction regime. In both cases, the optical gain of a gain-expanded system is substantially higher than obtainable from a conventional wiggler with the same acceptance or power output. Note, however, that since operation at high power in the low-extraction regime requires a high betatron phase advance per period (Eqn. 5-1), while operation at high extraction is possible even at small values of the betatron phase advance per period, the wiggler parameters in the high extraction regime can be chosen to yield a higher gain (which, from Eqn. 5-9, varies as $(\lambda_\beta \gamma)^{-1}$) than at low extraction.

The laser-induced energy spread and energy distribution functions are also important elements of operation in the high-extraction regime. For small initial emittances, the fluctuations in energy loss are remarkably small for operation on an even-π resonance $qL = \nu L = m \cdot 2\pi$, even for operation near saturation.

Figures 14-16 indicate that the computed energy loss distribution function at 8% mean energy loss for the wiggler in Table V have widths of less than 15% at $1 \cdot 10^{-8}$ cm-radians initial emittance less than 20% at $1 \cdot 10^{-7}$ cm-radians, and less than 40% at $1 \cdot 10^{-6}$ cm-radians.

The deterioration in energy spread with increasing initial emittance is a consequence of the random optical phase oscillations during the interaction, due to the electrons' initial betatron motion.[1] In general, the deterioration in energy spread is small so long as the initial emittance remains small compared to the emittance induced by the interaction. As an example, the laser-induced emittance for Figs. 14-16 is $8.5 \cdot 10^{-6}$ cm-radians; the figures indicate only a small effect on energy spread for initial emittances reduced from this number by a factor of 10.

In the low-extraction regime, the electrons make repeated pulses through the wiggler at emittances equal to or greater than the incremental laser induced emittance growth. In this case, the random phase oscillations caused by the initial betatron motion dominate and the laser-induced energy spread is large compared to the radiated energy. But in the high extraction regime, the time interval between shots can be chosen to permit the synchrotron radiation to damp the laser-induced emittance. If sufficient time is allowed between shots, the emittance will return to a small value between shots yielding a small spread in the radiated energy.

The actual radiated power and efficiency attainable in the high extraction regime will be determined by the single pass saturation characteristics and the damping required to control the laser-induced emittance and energy spread. As is apparent from Figures 14-16, the net betatron damping between such must be large enough to reduce the emittance by an order of magnitude or so between shuts,while sufficient energy damping must be provided to keep the accumulated energy spread within manageable limits. We note also that in a situation in which the spread in radiated energy per shot is small, the choice of synchrotron frequency can affect the energy distribution since the synchrotron phase advance between shots will determine the way in which the energy fluctuations accumulate in successive shots to determine the equilibrium distribution.

The possibilities for power output and efficiency in the high extraction regime can be illustrated by considering the performance attainable with the wiggler of Table V operated under the conditions of Figure 16, eg, with an emittance $\sim 1 \cdot 10^{-6}$ cm-radian. To limit the single shot and accumulated laser-induced energy spread we will assume betatron and synchrotron damping factors $e^{-\alpha_x T} \sim 1/\sqrt{10}$ and $e^{-\alpha_\varepsilon T} \sim 1/\sqrt{2}$. This betatron damping rate dumps the emittance by a factor of 10 between laser shots. Given an appropriate synchrotron phase advance, this choice of synchrotron damping limits the accumulated energy spread to 2 times the single pass energy spread. From Sands, the damping rates can be expressed as:

$$\alpha_x T \equiv (1-D)\frac{P_{sym}}{2E_o} T$$

$$\alpha_E T \equiv D\frac{P_{sym}}{2E_o} T$$

$$T \equiv \text{time between shots} \qquad (6\text{-}1)$$

Solution of equation (6-1) for D and T yield:

$$\begin{aligned} D &= -1.3 \\ P_s T/E_o &= 1.0 \quad . \end{aligned} \qquad (6\text{-}2)$$

With this choice of damping coefficients, the energy radiated as synchrotron radiation between passes is just equal to the electron energy. We then have, for the radiated power per electron $\langle P_{laser} \rangle$ and efficiency:

$$\begin{aligned} \langle P_{laser} \rangle &\sim \langle \delta \rangle \gamma_o mc^2 / T \\ \text{Efficiency} &\equiv \langle P_{laser} \rangle / P_{sym} \\ &= \langle \delta \rangle \gamma_o mc^2 / P_{sym} \cdot T \end{aligned} \qquad (6\text{-}3)$$

In the example under consideration, in which $T \cdot P_{synch}$ is equal to E_o, the efficiency is just $\langle \delta \rangle$. For the wiggler and condititons of Figure 16, in which the mean extracted energy $\langle \delta \rangle = 0.08$, the efficiency would be 8%. Larger efficiencies would require either an increase in the single pass extraction or a decrease in the time interval between shots.

The statistics for operation in the high extraction regime, and their implications for the storage ring energy aperture requirements, also follow from the choice of damping rates. If the laser

is fired at intervals of $2\pi M + \frac{\pi}{2}$ in synchrotron phase, where $M = 1,2,3,\ldots$, an electrons' energy deviation Δ_i on the ith shot can be expressed as:

$$\Delta_i = \delta_i - e^{-2\alpha_E T} \Delta_{i-2} \qquad (6\text{-}4)$$

where δ_i = laser induced change in energy on the ith shot

The absence of any terms involving δ_{i-1}, δ_{i-3}, δ_{i-5},... in Eqn. (6-4) is due to the quadrature relationship of energy fluctuations added to the electrons at synchrotron phases differing by 90°. Expressing Δ_{i-2} in (6-4) terms of δ_{i-2}, δ_{i-4},..., we obtain

$$\Delta_i = \delta_i - e^{-2\alpha_E T} \delta_{i-2} + e^{-4\alpha_E T} \delta_{i-4} - e^{-6\alpha_E T} \delta_{i-6} + \cdots \qquad (6\text{-}5)$$

The mean and standard deviation of Δ_i follow immediately from Eqn. (6-5) and the single pass statistics for δ_i. Specifically

$$\langle \Delta_i \rangle = \frac{1}{1 + e^{-2\alpha_E T}} \langle \delta_i \rangle \qquad (6\text{-}6)$$

$$\langle \Delta_i^2 \rangle - \langle \Delta_i \rangle^2 = \frac{1}{1 - e^{-2\alpha_E T}} \cdot \left[\langle \delta_i^2 \rangle - \langle \delta_i \rangle^2 \right]$$

In the example under consideration, in which $e^{-\alpha_E T} = 1/\sqrt{2}$, the standard deviation of the energy distribution of the circulating electrons in the ring would be larger only by a factor of $\sqrt{2}$ than the standard deviation of the electrons change in energy in a single pass through the wiggler as indicated in Figure 16.

The storage ring energy aperture requirements are defined by the probability density in the wings of the electrons' distribution. In the low extraction regime, the energy distribution was gaussian, requiring an energy aperture $\sim$ 4-6 times the standard deviation to secure an adequate lifetime. But in the high extraction regime, the existence of substantial damping between laser shots, and the existence of absolute upper and lower limits to the energy radiated in each shot, sets absolute upper limits to the electrons' deviation from the nominal energy. Assuming again a synchrotron phase advance between shots equal to $2\pi M + \frac{\pi}{2}$, the maximum possible energy deviation is:

$$\begin{aligned} \Delta \leq\ & \delta_{max}\left(1 + e^{-2\alpha_E T} + e^{-4\alpha_E T} + \cdots\right) \\ & - \delta_{min}\left(e^{-2\alpha_E T} + e^{-4\alpha_E T} + \cdots\right) \\ =\ & \frac{1}{1 - e^{-4\alpha_E T}}\left(\delta_{max} - e^{-2\alpha_E T}\,\delta_{min}\right) \end{aligned} \tag{6-7}$$

where δ_{max} $\equiv$ largest possible single pass energy change

δ_{min} = smallest possible single pass energy change.

Assuming the same energy damping $e^{-\alpha_E T} = 1/\sqrt{2}$ as in the rest of the example, and the energy distribution shown in Figure 16 for an emittance of $1 \cdot 10^{-6}$ cm-radians, we obtain:

$$\begin{aligned} \delta_{max} &= 0.11 \\ \delta_{min} &= 0.01 \end{aligned} \qquad (6\text{-}8)$$

$$\Rightarrow \Delta \leq 0.14$$

Since the laser can not drive electrons to energy deviations larger than this value, it would suffice to set the storage ring aperture just incrementally above this value. Note that the aperture implied by Eqn. (6-8) is less than twice the laser efficiency $< P_{laser} > / P_{synch} = 8\%$ computed for this example. By comparison, the attainment of long beam lifetimes in the low extraction regime would require an energy aperture approximation four times the desired efficiency (see Eqn. (5-17)).

Evidently the attainment of the aperture required for high efficiency operation would still be a limiting factor in high extraction operation. Although the 14% acceptance required in this example is smaller than the 32% acceptance required for the same efficiency in the low-extraction regime, it would still exceed by a factor of two the aperture of the most ambitious storage ring design developed to date. Probably the best performance which could be anticipated with present technology would be an ± 8% aperture, as in the LEDA design, from which a 4.5% efficiency might be attainable in the high extraction regime.

The requirement to restrict the repetition rate of the laser may also prove troublesome. The time scale for the device is set by the damping time of the ring, which is unlikely to fall below 1-10 milliseconds. For an oscillator with sufficiently high single pass gain, it might be adequate to Q-switch the cavity or to deflect the electron beam to terminate the pulse at saturation and to prevent oscillation during damping. In such a system, the rapid growth of the optical field in successive passes would maintain the emittance growth in each pass large enough to dominate the emittance generated in the preceeding pass. If only low gain is available, a multiple-pass resonator would presumably be required in which the cavity length could be set to separate the electron bunch and optical pulse for 10-100 orbits following each interaction. An independent evaluation of these measures will evidently be required to evaluate the practical prospects for operation in the high-extraction regime.

VII. SUMMARY

The development of the thin-lens model for gain-expanded wigglers has permitted the resolution of a number of fundamental questions concerning the optimization of parameters and ultimate limits to the gain, power and efficiency of gain-expanded storage ring free electron lasers.

In the low-extraction region, we find that laser power output will be ultimately limited by emittance growth. Efficiencies in excess of 10% can be achieved in principle by operating the wiggler at a large betatron phase advance per unit length. The use of gain expansion in a high power system can improve the gain by nearly an order of magnitude as compared to a system using conventional constant-period wigglers. Similar efficiencies can be obtained in the high extraction region, with the added benefit of reduced energy aperture requirements. In all cases, the attainment of high efficiency and power output require a large storage ring energy acceptance. The practical limit to the power output presently attainable in storage ring free electron lasers will likely be set by this parameter.

The relations observed in our numerical simulations between laser induced energy spread, emittance, and radiated energy are generally consistent with the approximate analytic expressions devised by Kroll and Rosenbluth.

REFERENCES

1. J. M. J. Madey and R. C. Taber, Phys. Quant. Elect. V.7 (Addison Wesley - 1980), p. 741.
   N. M. Kroll, P. L. Morton, M. N. Rosenbluth, J. N. Eckstein, and J. M. J. Madey, IEEE J. Quant. Elect. QE-17 (1981), p. 1496.
   J. M. J. Madey, "Numerical Interaction of Electron Trajectories in the Thin Lens Limit for a Gain-Expanded FEL," HEPL TN-82-1 (1982).
   N. M. Kroll and M. N. Rosenbluth, Journ. de Phys. Colloque 44, (1983) p. C1-85.
   J. M. J. Madey, Journ. de Phys. Colloque 44 (1983) p. C1-169.
2. AFOSR Contract # F49620-81-C-0077; Principal Investigator M. Rosenbluth, H. Vernon Wong and B. N. Moore.
3. J. M. J. Madey, "Design Notes for Medium Power Infrared FEL's," HEPL Report # 924, March 1983.
4. J. M. J. Madey, "Prospects for XUV Storage Ring Free Electron Lasers," HEPL Report No. 935 (November, 1983).
5. V. K. Neil, "Emittance and Transport of Electron Beams in a Free Electron Laser," Jason Technical Report JSR-79-10 (December, 1979).
   G. Dattoli, T. Letardi, J. M. J. Madey, and A. Renieri, ENEA C.R.E. Frascati Report # 83.13, submitted to IEEE J. Quant. Elect.

6. H. Wiedemann, J. de Phys. Colloque 44 (1983) p. C1-201.

7. A. Renieri, IEEE Trans. Nucl. Sci. 26 (1979)p. 3827.

8. T.I. Smith, J. M. J. Madey, L. R. Elias and D.A.G. Deacon, J. Appl. Phys. 50 (1974) p. 4580.

9. J. M. J. Madey, "Numerical Integration of Electron Trajectories in the Thin Lens Limit for a Gain Expanded FEL," HEPL TN-82-1 (1982).

10. M. Sands, "The Physics of Electron Storage Rings, An Introduction," SLAC-121 (1970).

11. K. L. Brown, "A First- and Second-Order Matrix Theory for the design of Beam Transport Systems and Charged Particle Spectrometers," SLAC-75 (June, 1982).

12. N. M. Kroll, and M. N. Rosenbluth, op. cit.

13. N. M. Kroll and M. N. Rosenbluth, private communication.

14. N. M. Kroll, P. L. Morton, M. N. Rosenbluth, J. N. Eckstein, J. M. J. Madey, op. cit.

15. N. M. Kroll and M. N. Rosenbluth, private communication.

16. R. Barbini, G. Dattoli, T. Letardi, A. Marino, A. Renieri, and G. Vignola, IEEE Trans. Nucl. Sci. 26 (1979) p. 3836.

17. N. M. Kroll, P.L. Morton, M. N. Rosenbluth, J. N. Eckstein and J. M. J. Madey, op. cit., p. 1501

18. N. M. Kroll and M. N. Rosenbluth, op.cit.

TABLE I

SRFEL PARAMETERS

	$E_o = \gamma_o mc^2$	nominal electron energy
	β	betatron function
	$A \equiv \pi\{x'^2_\beta \beta + \beta(x'_\beta - \beta' x_\beta/2\beta)^2\} \equiv$	emittance
	$\equiv$ area of x_β, x'_β phase ellipse	(π-cm-rad)
Wiggler	L	length
(each section)	λ_o	cell period
	$\tilde{\lambda} L_o$	betatron phase advance
	qL	optical phase advance
	X	oscillation amplitude for nominal orbit
	X'	transverse derivative of X
		dispersion function $\eta^2 \approx \frac{1}{\tilde{\lambda}^2} \frac{1-\beta_\parallel^2}{1-X'^2}$
(match section)	$\Delta\phi_m$	betatron phase advance in matching section
	$\Delta\psi_m$	optical phase advance in matching section
Ring	N_D	number of turns to damp
	D	damping partition parameter
	U^o_{syn}	fractional synchrotron energy loss/turn ($=N_D^{-1}$)
	U^o_{rf}, ω_{rf}	RF voltage and frequency
	α	momentum compaction
	L_r	length of ring
	$\Delta\phi_r$	betatron phase advance over ring
Laser field	ε	field amplitude
	ψ_o	initial optical phase
	λ	wavelength
	σ_θ	phase width (radians RF phase) for Gaussian pulse

TABLE II

NUMERICAL VERIFICATION OF GSE RELATIONS

$\langle E_2 \rangle$	$\frac{1}{2}\frac{\partial}{\partial E_o \langle E_1^2 \rangle}$	$\frac{1}{2}\frac{\partial}{\partial A_o \langle E_1 A_1 \rangle}$	$\langle A_2 \rangle$	$\frac{1}{2}\frac{\partial}{\partial A_o \langle A_1^2 \rangle}$	$\frac{1}{2}\frac{\partial}{\partial A_o \langle A_1 E_1 \rangle}$	$-\frac{\langle \Delta A \rangle}{\langle \Delta \delta \rangle}$
(1) $\tilde{\kappa}L = qL = 8\pi$	$\tilde{\kappa}\lambda_o = .2\pi$	L=20 m	$1 - X'^2 = .99$			$\lambda = 10^{-4}$cm
$-8.54 \pm .01 \times 10^{-11}$	$< 10^{-16}$	$-8.54 \pm .01 \times 10^{-11}$	$8.54 \pm .01 \times 10^{-15}$	$8.54 \pm .01 \times 10^{-15}$	$< 10^{-27}$	$1.00 \pm .001 \times 10^{-45}$
(2) $\tilde{\kappa}L = qL = \pi$	$\tilde{\kappa}\lambda_o = .02\pi$	L = 20 m	$1 - X'^2 = .5$			$\lambda = 10^{-4}$cm
$-6.10 \pm 0.1 \times 10^{-10}$	$.47 \pm .01 \times 10^{-10}$	$-6.58 \pm .01 \times 10^{-10}$	$6.57 \pm .01 \times 10^{-14}$	$6.58 \pm .01 \times 10^{-14}$	$< 10^{-20}$	$1.077 \pm .001 \times 10^{-4}$

TABLE III

MANLEY-ROWE RELATION AND a_s CORRECTION

($\tilde{\Lambda}L \equiv 10\,\pi$, $qL = 11\pi$, L=20m, λ_0=40 cm, $1-X'^2$=.9, $S=10^3$ watt/cm^2, λ= 1μm)

Phase of correction (relative to Eq. (2-7))	$-\langle\Delta A\rangle/\lambda\ \langle\Delta\delta\rangle$
$+\pi/2$	.977
0	1.006
$-\pi/2$	.978
$-\pi$	.948
no correction	.978

TABLE IV

COMPARISON OF EVEN-π and ODD-π WIGGLERS

($L=20m$, $1-X'^2=.9$, $\lambda_o\tilde{\lambda}=.2\pi$, $\sigma_\theta=10^{-4}$, $S=10^8$ watts/cm^2)

	$qL = \tilde{\pi}L = 8\pi$	$qL = \tilde{\pi}L = 7\pi$
Extracted Energy $-\langle\Delta\delta\rangle$	$.29 \times 10^{-5}$	$.30 \times 10^{-5}$
Energy spread σ_δ	$.20 \times 10^{-2}$	$.20 \times 10^{-2}$
Efficiency ratio	1.45	1.49
Mean Emittance $\langle A\rangle$	$.27 \times 10^{-6}$	$.29 \times 10^{-6}$

TABLE V

RADIATED ENERGY AS A FUNCTION OF OPTICAL POWER DENSITY

$S(watts/cm^2)$	$\langle\delta\rangle$
2×10^{6}	1.2×10^{-8}
2×10^{8}	1.2×10^{-6}
2×10^{10}	1.2×10^{-4}
2×10^{12}	1.2×10^{-2}
2×10^{13}	7.8×10^{-2}
2×10^{14}	7.7×10^{-2}

Wiggler Parameters:

$L = 20$ meters

$\lambda_o = 100$ cm

$qL = \lambda_o\tilde{\lambda} = 4\pi$

$X' = 3.16 \times 10^{-2}$

$\gamma_o = 1733.5$

$\lambda = 1\ \mu m$

FIGURE CAPTIONS

Figure 1: SRFEL Schematic

Figure 2: Model for FEL laser insertion. (a) Split-magnet design. (b) Thin lens wiggler section consisting of alternating magnets of focal lengths f_1, f_2 and thickness Δz. The bending field within the thin lenses has a linear transverse gradient. The nominal orbits are sawtooth functions.

Figure 3: The averaged trajectory $< x >$ for an arbitrary orbit.

Figure 4: The electron trajectory changes slope on entering the laser field. There is a smaller correction to its energy from the work done over the finite buildup length $\delta\ell$.

Figure 5: Convergence of Monte Carlo simulation. The separate simulations runs used different initial electron trajectories or different seed values for the stochastic initial optical phase. N_D = 1000 passes. ($qL = \tilde{\lambda}L = 8\pi$, $L \equiv 20$ m, $\lambda_o = 50$ cm, $X' = .1$, $\gamma_o = 767$, $D = .5$, short optical pulse $S = 2 \times 10^9$ watt/cm^2)

Figure 6: The equibrium energy distribution with the laser remains nearly gaussian after 40,000 passes (log scale). ($qL = \tilde{\lambda}L = 8\pi$, $L = 20$ m, $\lambda_o = 50$ cm, $X' = .1$, $\gamma_o = 767$, $D = -.5$, cw optical pulse $S = 2 \times 10^7$ watt/cm^2).

Figure 7: Energy distribution ($qL = \tilde{\chi}L = 8\pi$, $L = 20$ m, $\lambda_o = 50$ cm, $X' = .1$, $\gamma_o = 767$, $D = 0$, cw optical pulse $S = 10^8$ watt/cm^2). Within the gaussian envelope there are depleted regions.

Figure 8: Equilibrium emittance distribution ($qL = \tilde{\chi}L = 8\pi$, $L = 20$ m, $\lambda_o = 50$ cm, $X' = .1$, $\gamma_o = 767$, $D = -.25$, cw optical pulse $S = 2 \times 10^7$ watt/cm^2).

Figure 9: The energy spread is proportional to the extracted energy in the unsaturated regime. The slope is given by Eqn. (4-1).

Figure 10: The laser gain is saturated at the maximum allowed emittance of Eqn. (4-3). The unsaturated regime is described by Eqn. (4-2),(solid line).

Figure 11: The efficiency ratio versus damping partition for three cw optical power densities. A local maximum near $D = 0$ is a frequent feature at higher powers. ($qL = \tilde{\chi}L = 8\pi$, $L = 20$ cm, $\lambda_o = 50$ cm, $X' = .1$, $\gamma_o = 767$, cw optical pulses).

Figure 12: Efficiency ratio versus damping partition with short optical pulses. The gaussian width of the cw optical pulse was 2% of the corresponding electron longitudinal pulse shape. ($qL = \tilde{\chi}L = 8\pi$, $L = 20$ cm, $\lambda_o = 50$ cm).

Figure 13: Efficiency ratio for different values of $qL = \tilde{\lambda}$ and X'. (L = 20 m, λ_o = 50 cm, D = 0, short optical pulse S = 2×10^8 watt/cm^2, $\sigma_\theta = 10^{-4}$)

Figure 14: Final electron energy distribution for the wiggler of Table V at an optical power density of 2×10^{13} watt/cm^2 and an initial emittance equal to 1×10^{-8} π-cm-radians. The initial β-function is set equal to the wiggler's intrinsic β-function.

Figure 15: Same as figure 14, but with an initial emittance equal to 1×10^{-7} π-cm-radians.

Figure 16: Same as figure 14, but with an initial emittance equal to 1×10^{-6} π-cm-radians.

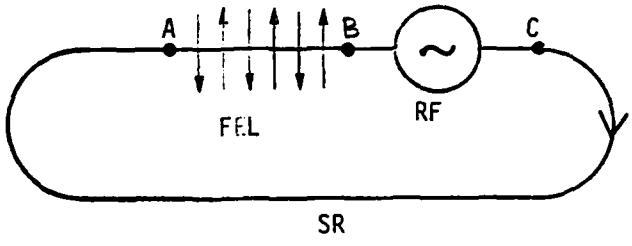

Figure 1

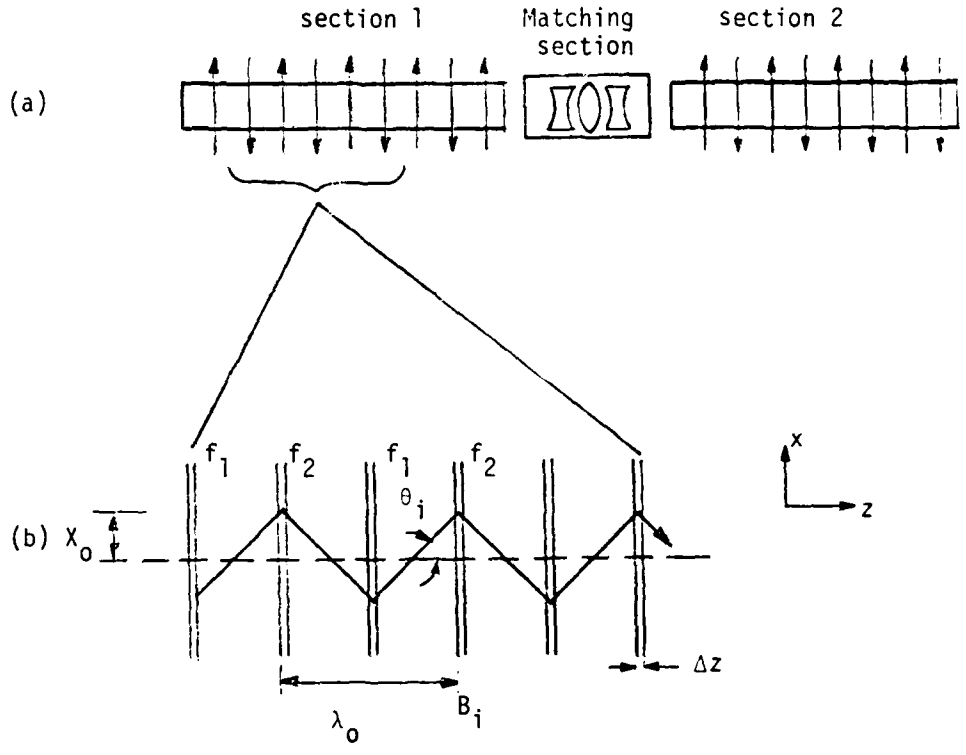
section 1
Matching section
section 2
(a)
(b) X_o
f_1
f_2
f_1
f_2
θ_i
x
z
Δz
λ_o
B_i

Figure 2

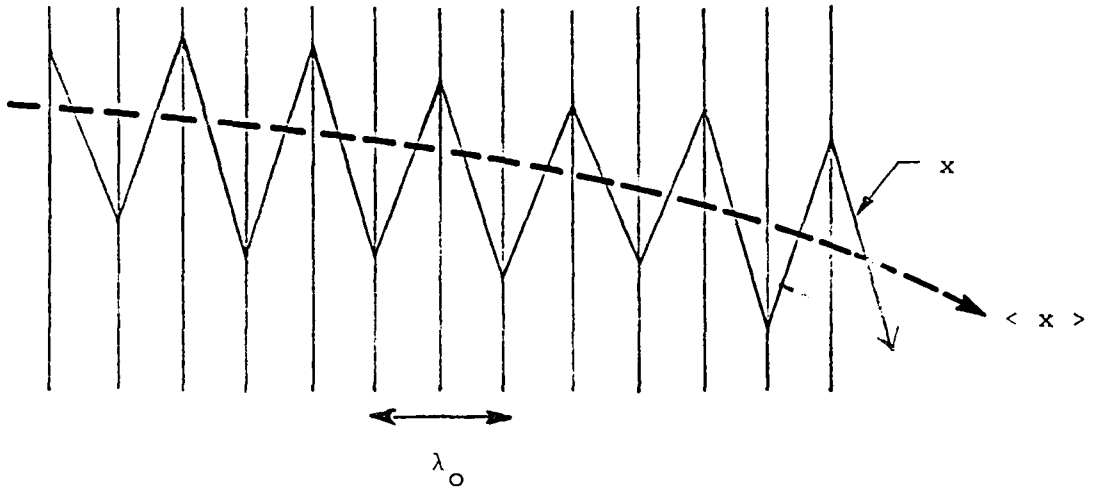

Figure 3

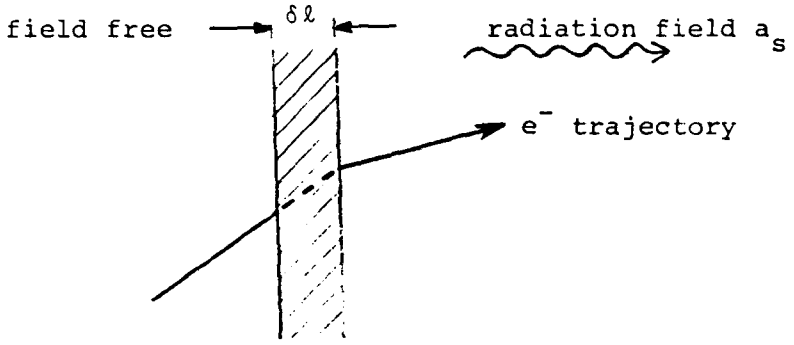

Figure 4

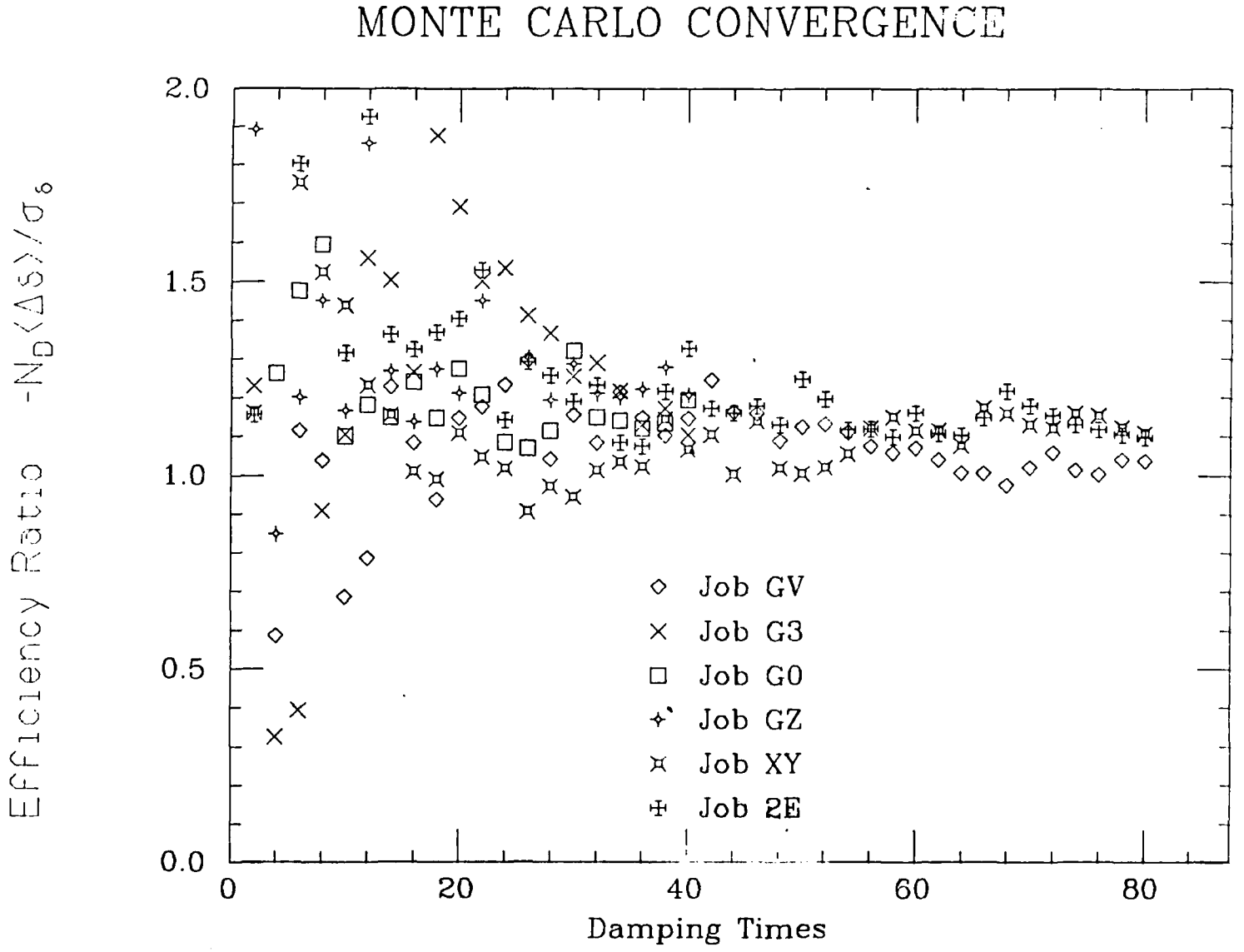
MONTE CARLO CONVERGENCE
Efficiency Ratio -$N_D\langle\Delta s\rangle/\sigma_\delta$
2.0
1.5
1.0
0.5
0.0
0
20
40
60
80
Damping Times
Job GV
Job G3
Job G0
Job GZ
Job XY
Job 2E

Figure 5

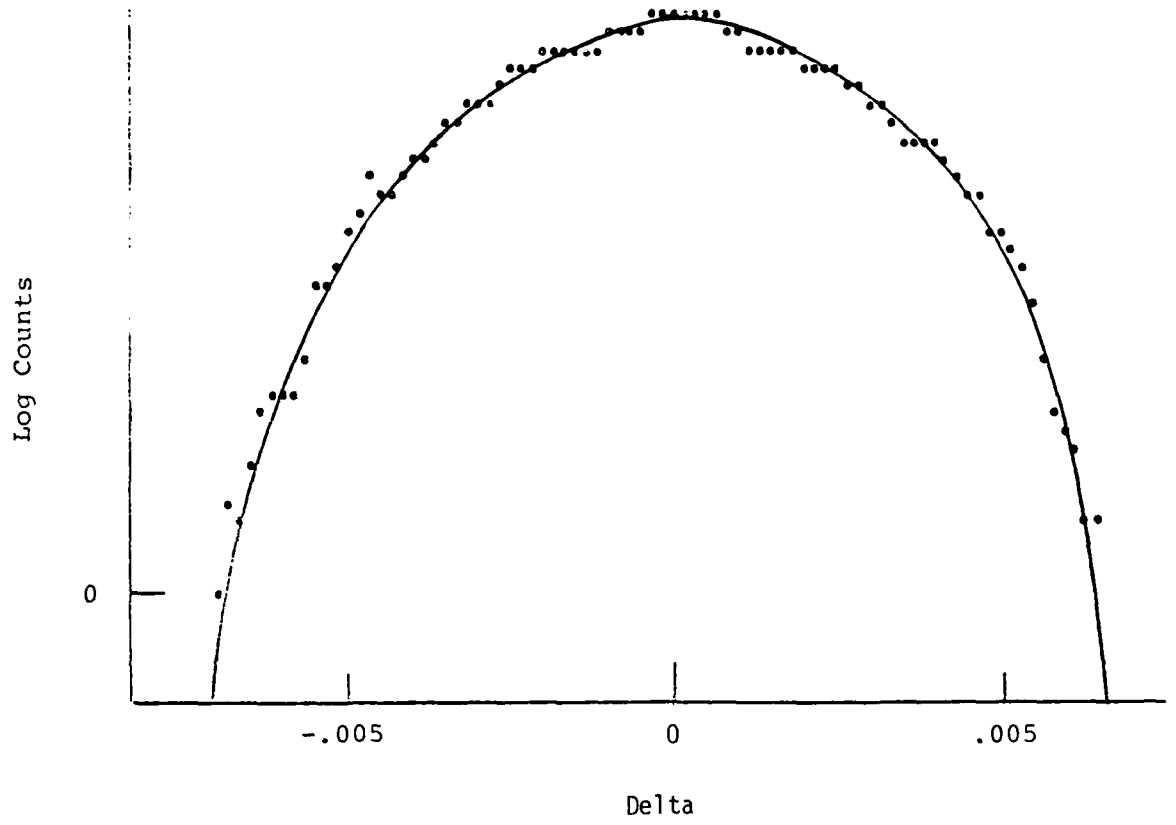

Figure 6

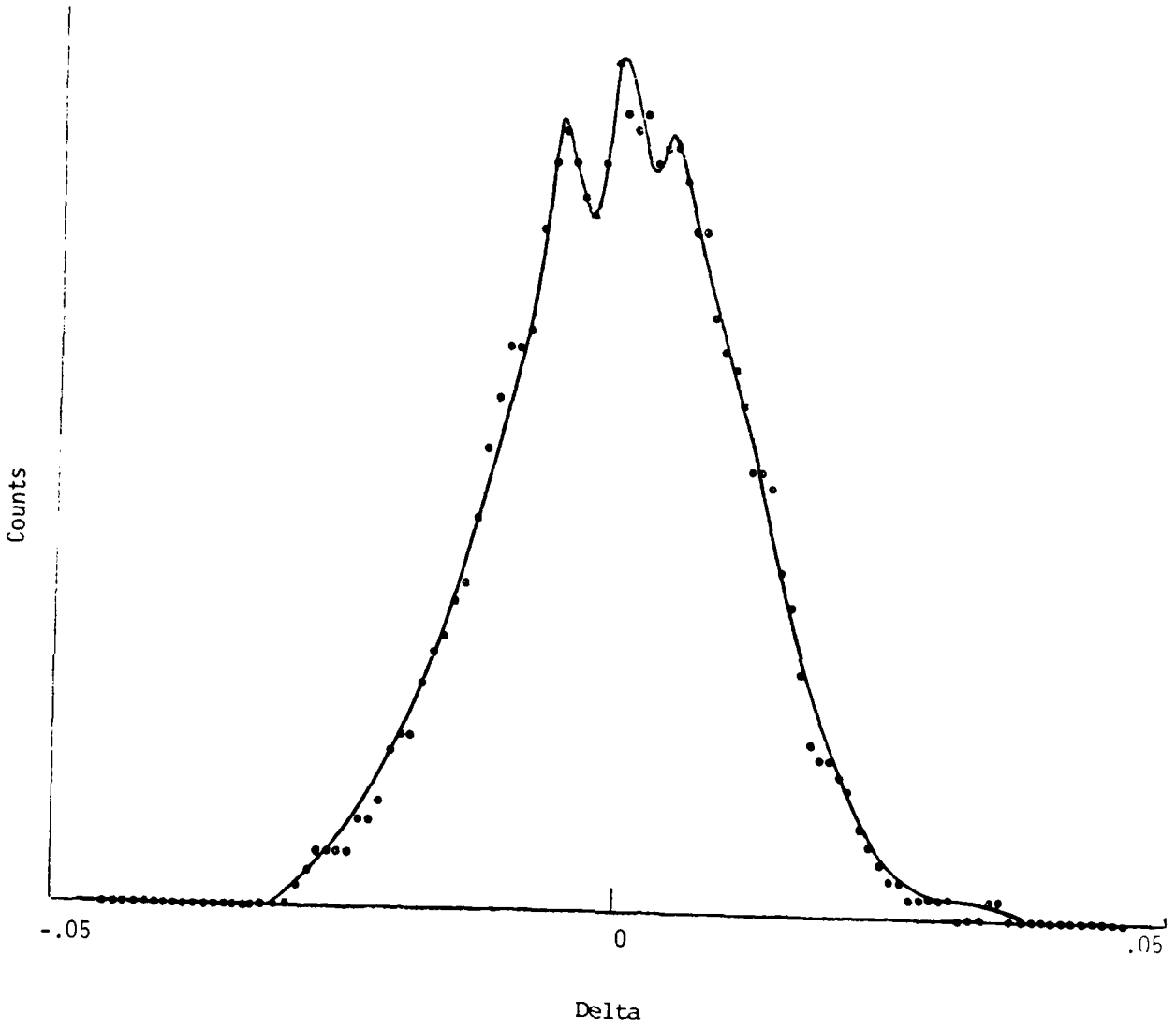

Figure 7

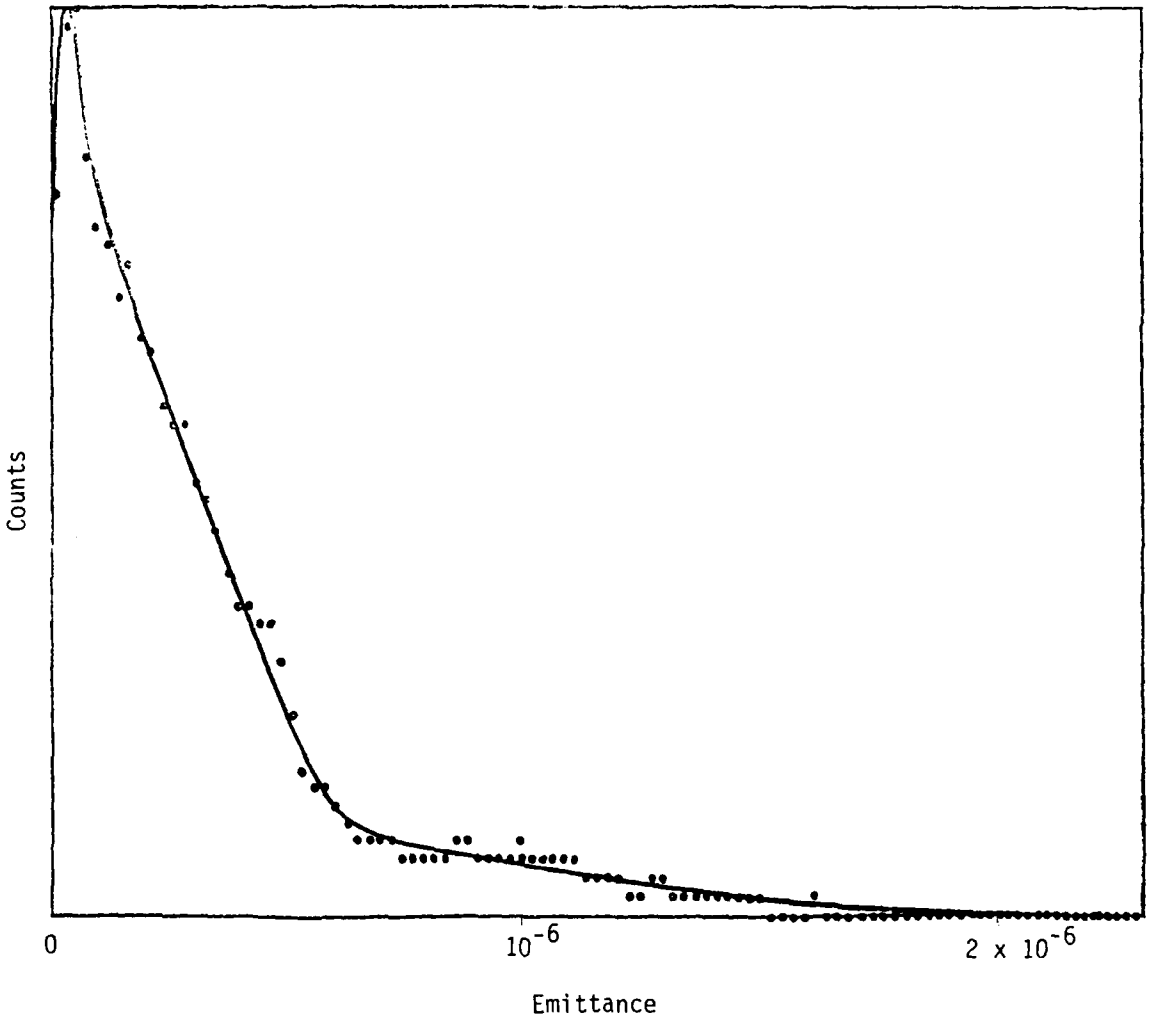

Figure 8

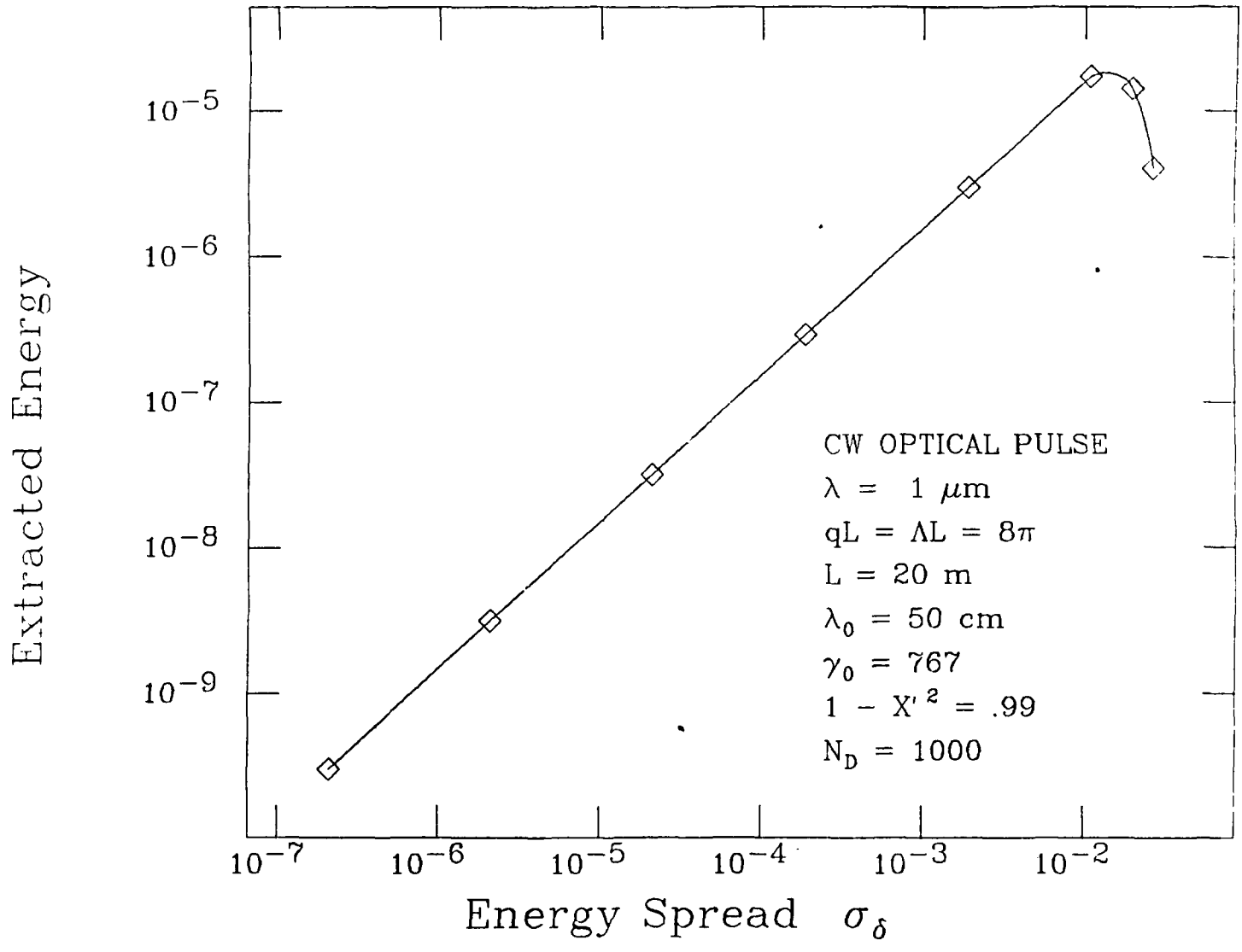
Extracted Energy
10^{-5}
10^{-6}
10^{-7}
10^{-8}
10^{-9}
CW OPTICAL PULSE
λ = 1 μm
qL = ΛL = 8π
L = 20 m
λ_0 = 50 cm
γ_0 = 767
1 - X'^{2} = .99
N_D = 1000
10^{-7}
10^{-6}
10^{-5}
10^{-4}
10^{-3}
10^{-2}
Energy Spread σ_δ

Figure 9

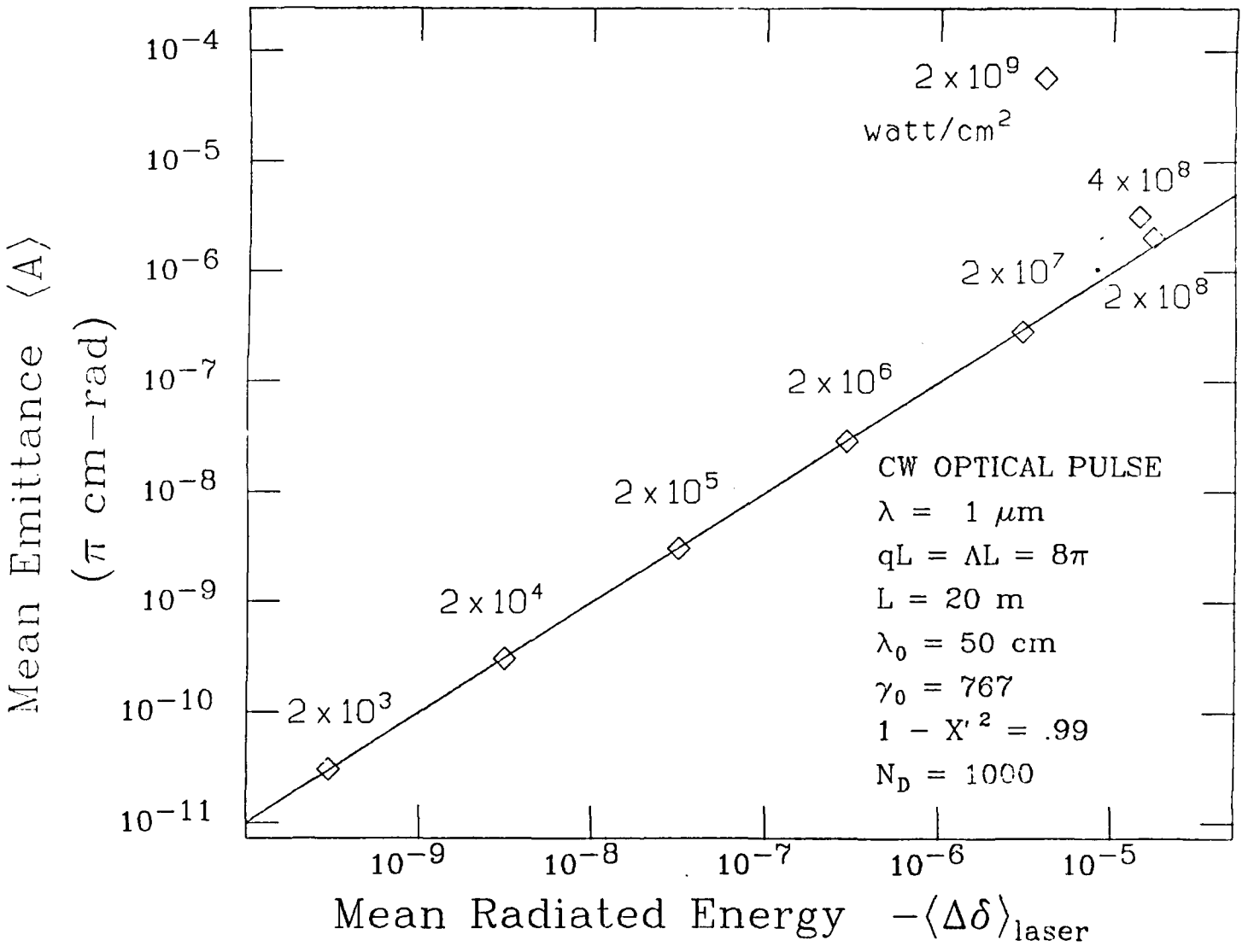
Mean Emittance ⟨A⟩
(π cm−rad)
10^−4
10^−5
10^−6
10^−7
10^−8
10^−9
10^−10
10^−11
2 x 10^9 ◇
watt/cm^2
4 x 10^8
2 x 10^7
2 x 10^8
2 x 10^6
2 x 10^5
2 x 10^4
2 x 10^3
CW OPTICAL PULSE
λ = 1 μm
qL = ΛL = 8π
L = 20 m
λ0 = 50 cm
γ0 = 767
1 − X'^2 = .99
N_D = 1000
10^−9
10^−8
10^−7
10^−6
10^−5
Mean Radiated Energy −⟨Δδ⟩laser

Figure 10

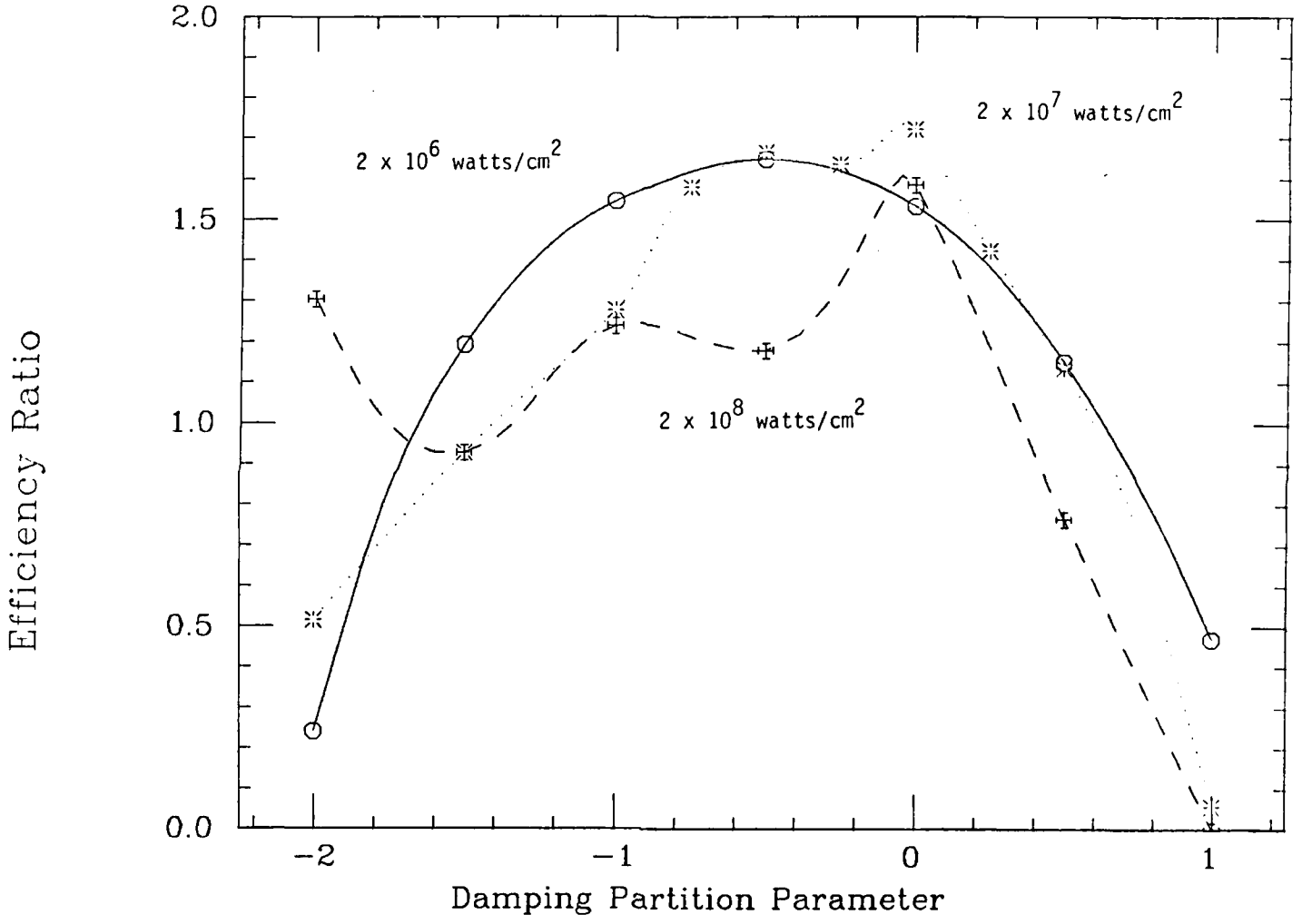
2.0
1.5
1.0
0.5
0.0
Efficiency Ratio
2 x 10^6 watts/cm^2
2 x 10^7 watts/cm^2
2 x 10^8 watts/cm^2
−2
−1
0
1
Damping Partition Parameter

Figure 11

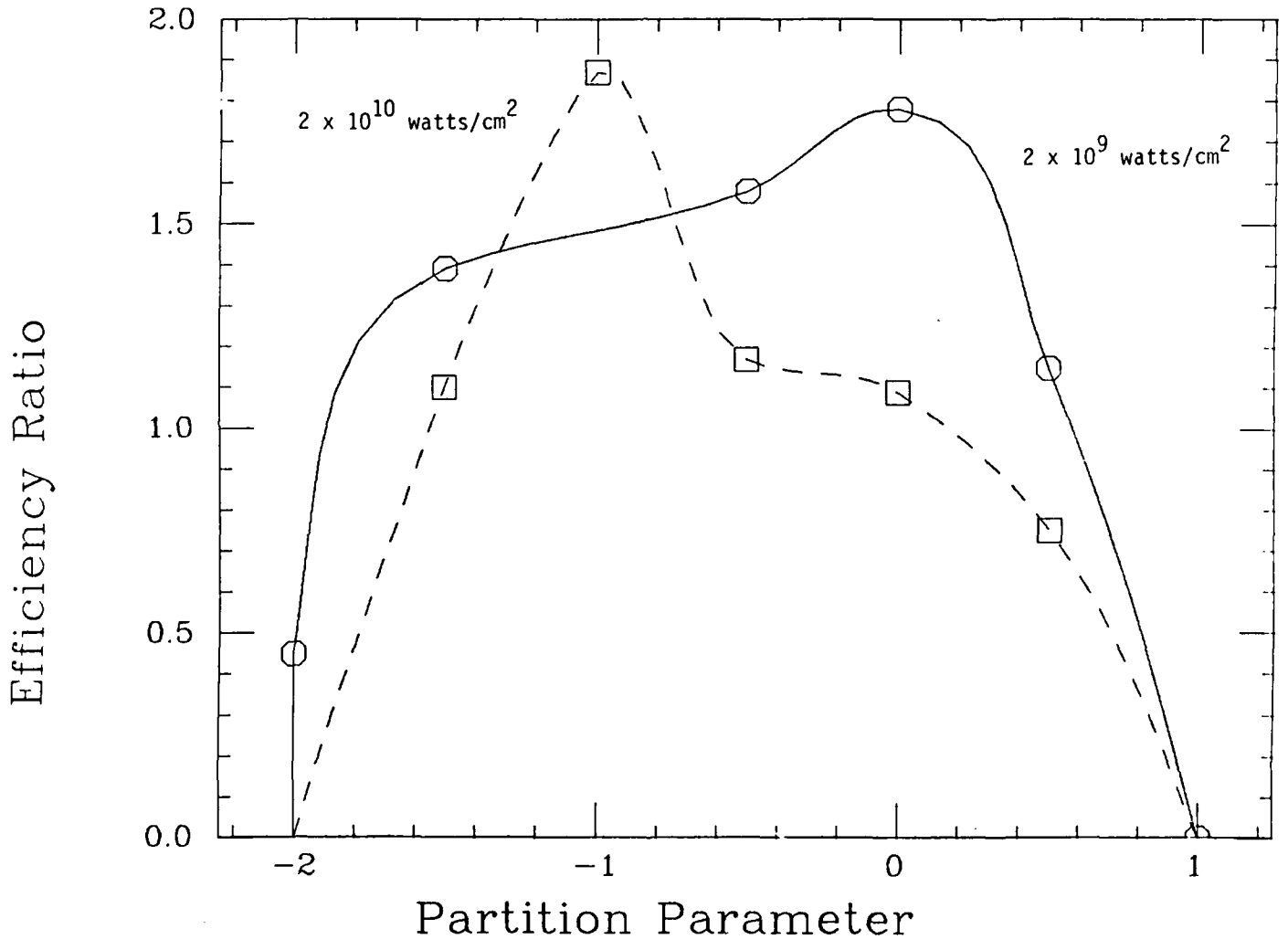
2.0
1.5
1.0
0.5
0.0
Efficiency Ratio
2 x 10^10 watts/cm^2
2 x 10^9 watts/cm^2
−2
−1
0
1
Partition Parameter

Figure 12

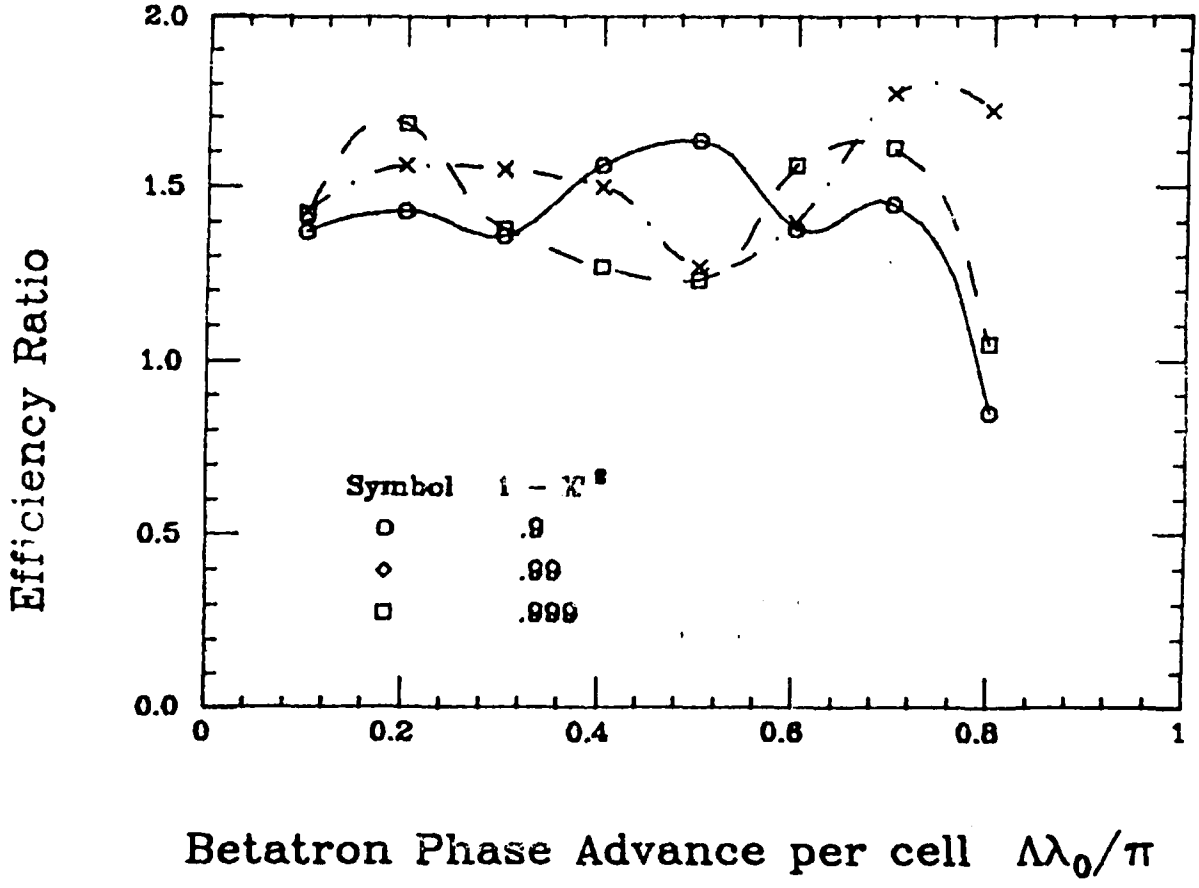
2.0
1.5
1.0
0.5
0.0
0
0.2
0.4
0.6
0.8
1
Efficiency Ratio
Symbol
1 - K²
.9
.99
.999
Betatron Phase Advance per cell Λλ0/π

Figure 13

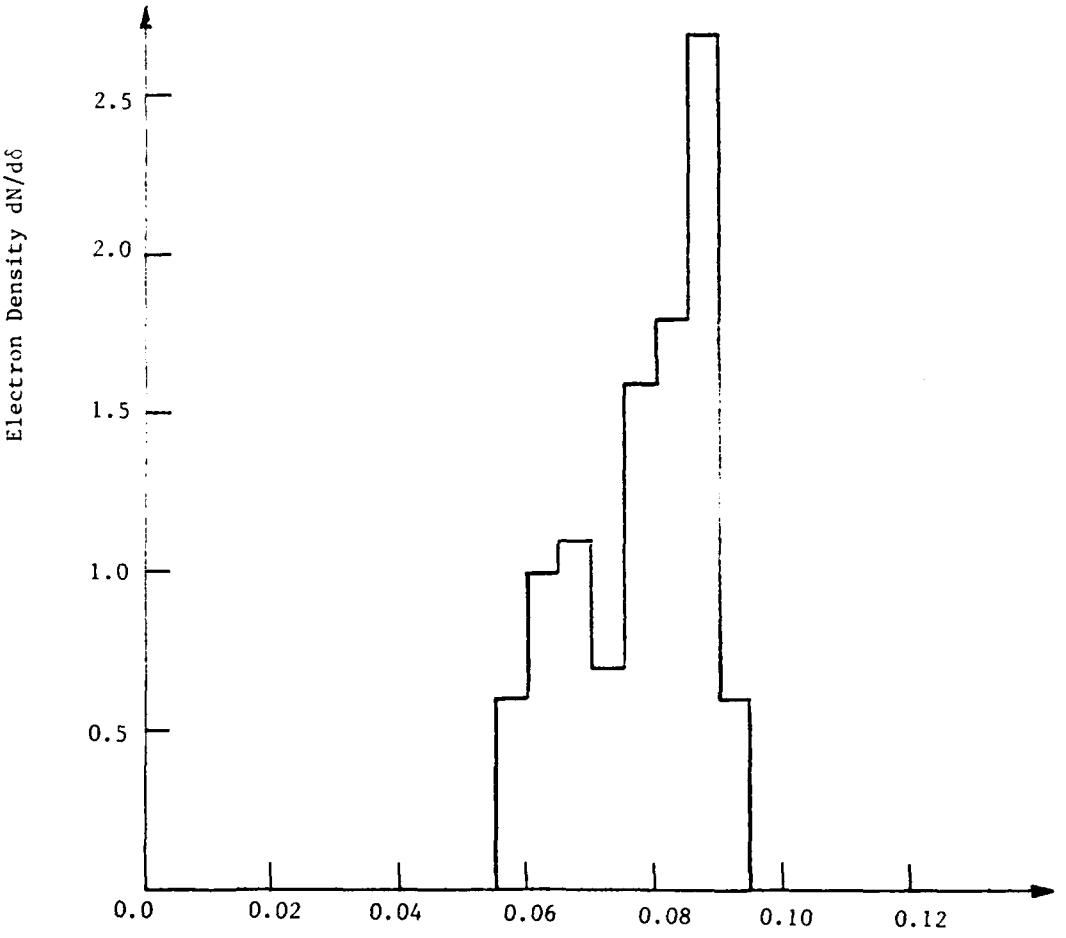
Electron Density dN/dδ
2.5
2.0
1.5
1.0
0.5
0.0
0.02
0.04
0.06
0.08
0.10
0.12
Normalized Energy Loss δ

Figure 14

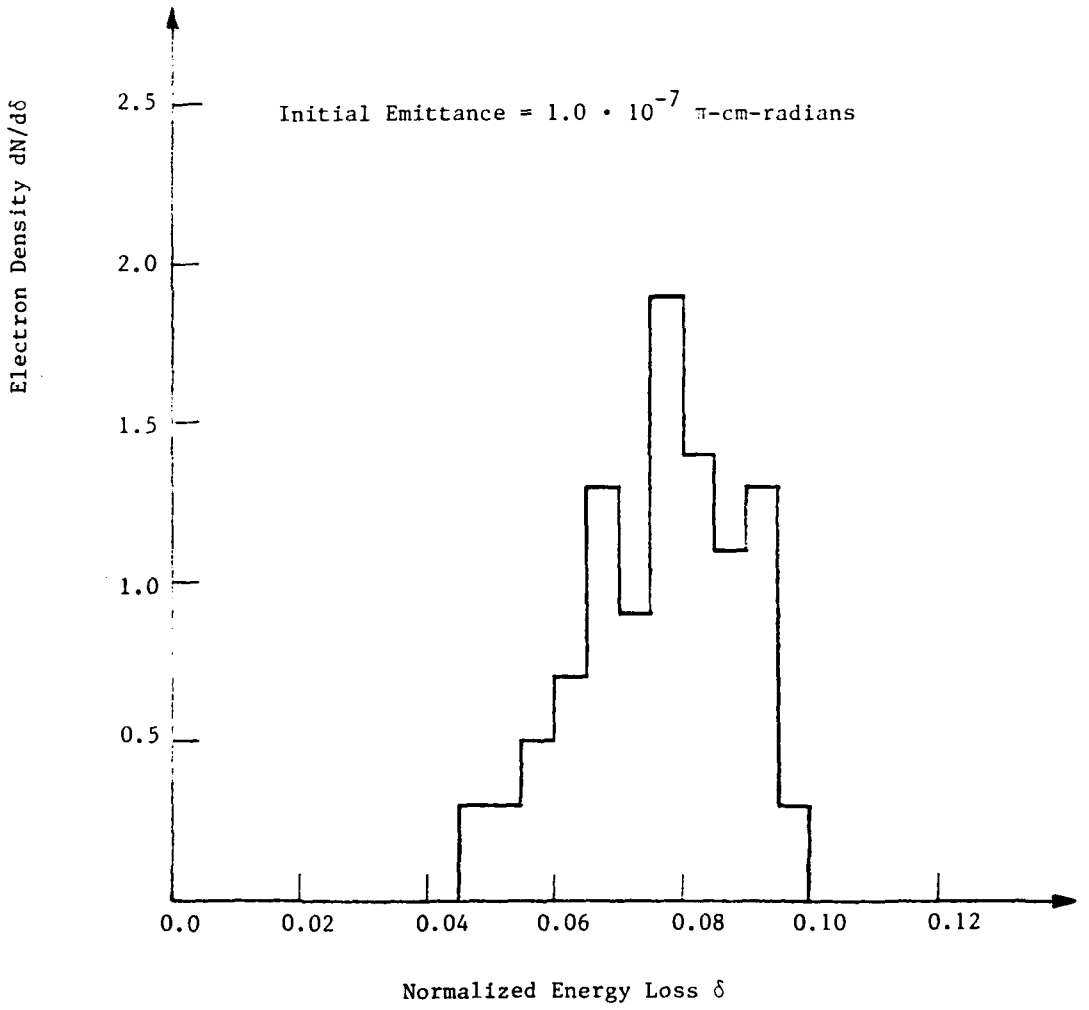
Initial Emittance = 1.0 • 10^-7 π-cm-radians
Electron Density dN/dδ
2.5
2.0
1.5
1.0
0.5
0.0
0.02
0.04
0.06
0.08
0.10
0.12
Normalized Energy Loss δ

Figure 15

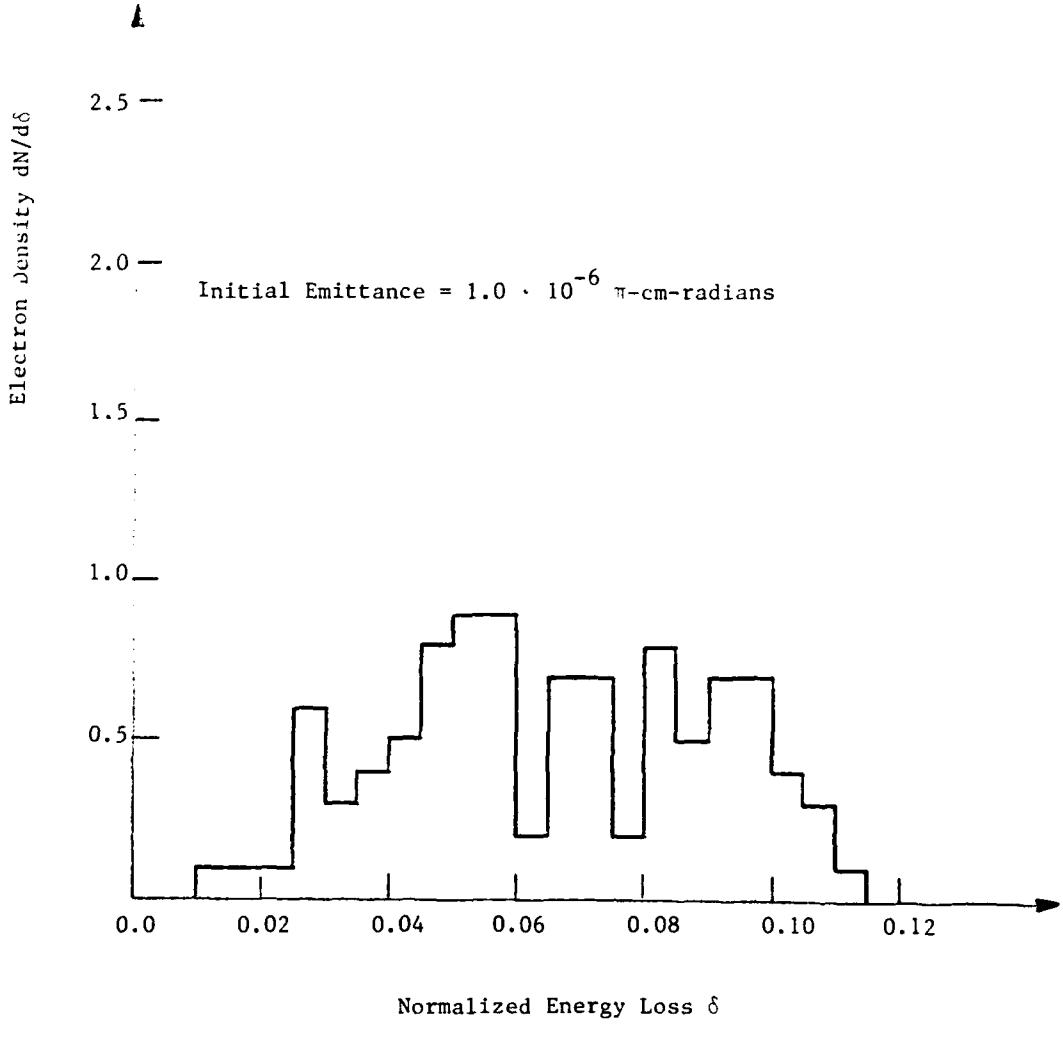
Electron Density dN/dδ
2.5
2.0
1.5
1.0
0.5
Initial Emittance = 1.0 · 10^-6 π-cm-radians
0.0
0.02
0.04
0.06
0.08
0.10
0.12
Normalized Energy Loss δ

Figure 16